JCI The Journal of Clinical Investigation

# STAT3-enhancing germline mutations contribute to tumor-extrinsic immune evasion

Daniel Kogan, … , Christian Faul, Vijay Kumar Ulaganathan

*J Clin Invest.* 2018. https://doi.org/10.1172/JCI96708.

**Concise Communication** In-Press Preview **Genetics** **Oncology**

Immune evasion and the suppression of anti-tumor responses during cancer progression are considered hallmarks of cancer and are typically attributed to tumor-derived factors. Although the molecular basis for the crosstalk between tumor and immune cells is an area of active investigation, whether host-specific germline variants can dictate immunosuppressive mechanisms has remained a challenge to address. A commonly occurring germline mutation (c.1162G>A/rs351855 G/A) in the *FGFR4* (CD334) gene enhances STAT3 signaling and is associated with poor prognosis and accelerated progression of multiple cancer types. Here, using rs351855 single nucleotide polymorphism (SNP) knock-in transgenic mice and *Fgfr4* knockout mice, we reveal the genotype-specific gain of immunological function of suppressing the CD8/$CD4^+FOXP3^+CD25^{+ve}$ regulatory T cell ratio in vivo. Furthermore, using knock-in transgenic mouse models for lung and breast cancers, we establish the host-specific tumor-extrinsic functions of STAT3-enhancing germline variants in impeding the tumor infiltration of CD8 T cells. Thus, STAT3-enhancing germline receptor variants contribute to immune evasion through their pleiotropic functions in immune cells.

**Find the latest version:**

https://jci.me/96708/pdf

# STAT3-enhancing germline mutations contribute to tumor-extrinsic immune evasion

**Daniel Kogan[1], Alexander Grabner[2], Christopher Yanucil[3], Christian Faul[3] & Vijay Kumar Ulaganathan[4]***

[1]Technische Universität München, Arcisstraße 21, München 80333, Germany, [2]Division of Nephrology, Department of Medicine, Duke University Medical Center, Duke University, Durham, NC 27705, USA, [3]Division of Nephrology, Department of Medicine, The University of Alabama at Birmingham, Birmingham, AL 35233, USA, [4] Max Planck Institute of Biochemistry, Department of Molecular Biology, Am Klopferspitz 18, 82152, Martinsried, Germany

* Corresponding author

**Immune evasion and the suppression of anti-tumor responses during cancer progression are considered hallmarks of cancer and are typically attributed to tumor-derived factors. Although the molecular basis for the crosstalk between tumor and immune cells is an area of active investigation, whether host-specific germline variants can dictate immunosuppressive mechanisms has remained a challenge to address. A commonly occurring germline mutation (c.1162G>A/rs351855 G/A) in the *FGFR4* (CD334) gene enhances STAT3 signaling and is associated with poor prognosis and accelerated progression of multiple cancer types. Here, using rs351855 single nucleotide polymorphism (SNP) knock-in transgenic mice and *Fgfr4* knock-out mice, we reveal the genotype-specific gain of immunological function of suppressing the CD8/CD4$^{+}$FOXP3$^{+}$CD25$^{+ve}$ regulatory T cell ratio in vivo. Furthermore, using knock-in transgenic mouse models for lung and breast cancers, we establish the host-specific tumor-extrinsic functions of STAT3-enhancing germline variants in impeding the tumor infiltration of CD8 T cells. Thus, STAT3-enhancing germline receptor variants contribute to immune evasion through their pleiotropic functions in immune cell**

## Introduction

Immune evasion is considered the hallmark of cancers (1). Strategies that restore the capacity of the immune system to recognize and eliminate malignant cells have produced clinical benefits. However, due to a dearth of predictive biomarkers for patient stratification, only one-third of all patients are responsive to treatment (2). Immune evasion by tumor tissues has been the major bottleneck in the development of therapeutically effective anticancer strategies. The prominent mechanisms by which tumors evade immune attack include the evolution of tumor cell variants that are resistant to immune effectors and the progressive formation of an immune suppressive microenvironment within the tumor that impedes the infiltration of anti-tumor effector cells. While a greater emphasis has been placed on understanding the function of tumor-intrinsic somatic heterogeneity or the tumor-induced microenvironment in evading immune surveillance, the role played by tumor-extrinsic host-specific genetic heterogeneity in modulating the anti-tumor immune response is poorly understood and remains challenging to address.

An attribute common to all cancers is the presence of numerous cell types, including bone marrow-derived inflammatory cells, lymphocytes, fibroblastic cells and the extracellular matrix composed of collagen and proteoglycans. Importantly, of diverse assemblages of tumor cell infiltrates, cytotoxic and regulatory T lymphocytes within the tumors are often the crucial factors that determine the outcomes of anticancer therapy (3, 4). For example, the increased T cell numbers, particularly an increased ratio of CD8/ FOXP3+ regulatory T cells ($T_{REGS}$) within the tumor microenvironment (TME), predict a favorable therapeutic response, whereas severe lymphopenia negatively impacts the chemo- and immunotherapy response (5). It is well recognized that while the host immune system can recognize and reject cancerous cells, it can also mold the somatic heterogeneity of tumors by assisting in the generation of immune-resistant tumor variants (6). Various mechanisms exist, such as the immunoediting whereby primary tumor rejection is rendered compromised and ineffective by the inhibition of cytotoxic CD8 T cell infiltration or viability in the tumor microenvironment. An imminent question thus arises: Can individual-specific heritable genetic variants regulate immune homeostasis such that immune surveillance is impaired in a host-dependent manner irrespective of the nature of oncogenic onslaught? Here, we attempted to address this question by dissecting the tumor-extrinsic immunological function of signal transducer and activator of transcription 3 (STAT3)-enhancing germline receptor variants in shaping the tumor microenvironment. Many of the genes that have been studied to modulate immune responses have variants that occur in frequencies ranging from rare (<1%) to common (>10%) in the general population. There are approximately 907.3 million single-nucleotide polymorphisms (SNPs) catalogued in the Single Nucleotide Polymorphism Database (dbSNP) build 150 (Feb 3, 2017), and it is practically impossible to systemically evaluate all polymorphic SNPs in the human genome through association studies alone. Here, we demonstrate for the first time that by examining the cancer-associated germline receptor variants that enhance the amplitude of STAT3 signaling in a genotype-dependent manner (7), potential individual-specific modulators of cancer immune surveillance can be systematically evaluated. Amplified STAT3 signaling is pro-mitotic in cancer cells, whereas studies using targeted ablation of STAT3 signaling in immune cells, such as dendritic cells, CD8 T cells, regulatory T cells, NK cells (8) and macrophages (9-11), establish the immunosuppressive properties of constitutively activated STAT3. We hypothesized that STAT3-enhancing germline variants are potentially the tumor-extrinsic germline-encoded determinants of immune evasion in the tumor microenvironment (TME). Our work provides valuable insights into the predictive value of host-specific STAT3-enhancing germline variants in impeding the immune cell infiltration of tumors.

## Results and Discussion

To identify all single nucleotide polymorphism (SNP) variants that create membrane-proximal tyrosine-based STAT3 docking motifs, we performed a comprehensive computational analysis of all publicly available human genotyping datasets viz., 1000 genomes phase 3 (12), the Catalogue of Somatic Mutations in Cancer (COSMIC) (13), the Cancer Cell Line Encyclopedia (CCLE) (14), the Single Nucleotide Polymorphism Database (dbSNP) (15), the Exome Aggregation Consortium (ExAC.r0.3) (16), the international haplotype map (HAPMAP) (17), the United States National Cancer Institute (NCI) 60 human tumor cell line (NCI-60) exomes (18), the Cancer Genome Atlas (TCGA) (19) and the whole genome sequences of healthy elderly people (Wellderly) (20) using our new python-based algorithm

called the Transmembrane Protein Sequence Variant Identifier (TraPS-VarI) (21). Of approximately one billion human variants analyzed, we identified SNPs in the human variome (Supplemental Table 1; supplemental material available online; https://vj-ulaganathan.github.io/) that create membrane-proximal STAT3 binding sites in juxtamembrane segments. Interestingly, a large majority of these rare SNPs in type I membrane proteins exhibited expression patterns restricted either to professional antigen presenting cells, namely, CD115+ Ly6c+ MHCII+ monocytes, CD115+ F4/80lo CD11c+ MHCII+ SiglecF- macrophages, CD45+ CD11b+ CD11c+ MHCII+ dendritic cells or immunosuppressive CD3+CD4+CD25+FOXP3+ regulatory T cells (Supplemental Table. 1, Supplemental Figure 1A, B, C). The SNP allele rs351855-A encoding the fibroblast growth factor receptor 4 variant (FGFR4 p.Gly388Arg) is the only commonly occurring STAT3-enhancing receptor variant with a minor allele frequency of 0.3 in the general population. Among the immune cells profiled, FGFR4 (alias CD334) was highly expressed in CD4+CD25+FOXP3+ regulatory T cells ($T_{REGS}$) (Figure 1A). Using FOXP3-GFP knock-in reporter mice (22), we found that protein levels of FGFR4 in CD4+CD25+FOXP3+ or CD4+GITR+FOXP3+ $T_{REGS}$ populations are elevated when $T_{REGs}$ are resident in the lymph nodes (Figure 1B, Supplemental Figure 2). Here, using transgenic rs351855 SNP knock-in mice (homozygous for minor allele rs351855-A denoted hereafter by $Fgfr4^{rs351855\text{-}A/A}$) and its wild-type littermates (homozygous denoted by $Fgfr4^{rs351855\text{-}G/G}$), we asked whether STAT3-enhancing germline variants can shape the tumour microenvironments pleiotropically independent of the cancer types. We first ascertained that the minor allele variant rs351855-A was functional in $T_{REGS}$ as indicated by elevated levels of 705-tyrosine phophorylated STAT3 (pY705) (Supplemental Figure 3A, B, C, D) in $Fgfr4^{rs351855\text{-}A/A}$ mice. No obvious differences were detected when we monitored $Fgfr4^{rs351855\text{-}A/A}$ and $Fgfr4^{rs351855\text{-}G/G}$ knock-in mice at 5-6 months of age by assessing the proportions of monocytes/macrophages, B and T lymphocytes in lymphoid compartments, including bone marrow, thymus, blood, lymph nodes and spleen (Supplemental Figure 4A, B, C). Likewise, analyses for the proportions of NK cells and TCRγδ+ T cells in the thymus, spleen and lymph nodes of $Fgfr4^{rs351855\text{-}G/G}$ and $Fgfr4^{rs351855\text{-}A/A}$ mice (Supplemental Figure 5A, B) showed no significant differences between the two genotypes. However, the numbers of $CD8^{+ve}$ T cells were significantly decreased in the thymus, blood, lymph nodes and spleens of $Fgfr4^{rs351855\text{-}A/A}$ mice compared to those of the wild-type $Fgfr4^{rs351855\text{-}G/G}$ littermates (Figure 2A, Supplemental Figure 6A, B). The suppressed levels of $CD8^{+ve}$ T cells in $Fgfr4^{rs351855\text{-}A/A}$ genotypes appeared as a systemic trait, since lower levels were also found in the non-lymphoid organs analyzed, including parenchymal tissues such as lung and mammary tissue pads (Figure 2B). On the other hand, the quantification of $FOXP3^{+}CD25^{+ve}$ T cells ($T_{REGs}$) revealed a significant increase in $T_{REGs}$ under unchallenged homeostasis conditions in healthy adult mice (Figure 2C, Supplemental Figure 6C). Concordantly, the levels of *Foxp3* and *Il10* transcripts were significantly elevated, while the levels of *Cd8* mRNA transcripts were decreased in the spleens of $Fgfr4^{rs351855\text{-}A/A}$ mice (Supplemental Figure 7A, B, C), further supporting a general decrease in the $CD8/T_{REGs}$ ratio in vivo. Interestingly, immunophenotyping analyses of wild-type (*Fgfr4*+/+) and FGFR4-deficient (*Fgfr4*-/-) mice showed no significant alterations in the $CD8{:}T_{REGs}$ ratio (Figure 2D, E) or other immune cells analyzed, including NK cells, TCRγδ+ T cells, B cells and macrophages (Supplemental Figure 8A, B, C) either in lymphoid or in parenchymal organs (data not shown).

To functionally consolidate our findings, we determined that an increase in STAT3 phosphorylation (pSTAT3) at Y705 in $T_{REGs}$ resulted in enhanced proliferation and suppressive functions of $T_{REGs}$. Isolated $T_{REGs}$ from *Fgfr4*$^{rs351855\text{-}A/A}$ mice exhibited a higher proliferation rate than the *Fgfr4*$^{rs351855\text{-}G/G}$ $T_{REGs}$, as shown by the eFluor670 dilution assay performed on CD3/CD28 activated cells *ex vivo* (Figure 3A), supporting STAT3-associated $T_{REG}$ proliferative function. However, we did not observe a similar increase in the proliferative potential of *Fgfr4*$^{rs351855\text{-}A/A}$ $CD8^{+ve}$ T cells. To assess if an increase in $T_{REGs}$ may play a role in the suppression of CD8 lymphocytes in *Fgfr4*$^{rs351855\text{-}A/A}$ mice, the functional capacities of $CD4^{+}CD25^{+}$ $T_{REGs}$ of either genotype in suppressing the expansion of $CD8^{+ve}$ T cells *ex vivo* were determined by in vitro activated co-cultivation assays. Three days post co-cultivation, $T_{REGs}$ derived from the spleens of *Fgfr4*$^{rs351855\text{-}A/A}$ mice suppressed the expansion of CFSE-labelled $CD8^{+ve}$ T cells to a significantly larger extent than the splenic-*Fgfr4*$^{rs351855\text{-}G/G}$ $T_{REGs}$ (Figure 3B). To some degree, the suppression was dependent on interleukin 10 (IL10), since the presence of neutralizing IL10 mAb in the co-cultures, particularly in higher CD8:$T_{REGs}$ ratios (32:1, 16:1), led to similar suppressive capacities by both genotypes (Supplemental Figure 9). IL10 signals primarily by inducing the tyrosine phosphorylation of STAT3 (pSTAT3 (Y705)) via the STAT3 docking sites in the cytoplasmic domains of IL10R (23). Therefore, we conclude that the synergistic action of the rs351855-A allele with IL10 signaling explains the enhanced suppressive functions of $T_{REGS}$ in *Fgfr4*$^{rs351855\text{-}A/A}$ knock-in mice. Thus, under healthy homeostatic conditions, a germline-encoded increase in basal pSTAT3 (Y705) levels in $T_{REGS}$ leads to a systemic decrease in the CD8:$T_{REG}$ ratio. This finding suggests that alterations in the CD8:$T_{REGs}$ ratio in vivo are mechanistically linked to the presence of the minor allele rs351855-A and are not determined by the activity of FGFR4. The STAT3-enhancing gain of function by the minor allele of rs351855 is independent of the extracellular or intracellular domains of FGFR4 and is mediated by the membrane-proximal STAT3 docking site in the juxtamembrane segment of the FGFR4 p.Gly388Arg variant (24). We therefore attribute the genotype-dependent systemic suppression of the CD8:$T_{REG}$ ratio to the pleiotropic effect of STAT3-enhancing gain of function by the SNP rs351855-A. Disruption of the STAT3 membrane-recruitment event by the depletion of FGFR4 in the *Fgfr4-/-* mice abolished the SNP-specific gain of the immunological phenotype (Figure 3C).

To determine whether STAT3-enhancing germline variants mediate a tumor-extrinsic immune evasive pleiotropic phenotype, we generated genetically engineered SNP knock-in mouse models (GEKIMM) for breast and lung cancers (see methods). As expected, although the tumor incidence rates in both the disease models were not dramatically altered, the tumor burden and progression were significantly elevated in animals expressing the minor allele variant rs351855-A (25). Flow cytometric analysis of the age- and gender-matched cohorts of knock-in transgenic mouse models for breast (26) (*Fgfr4*$^{rs351855\text{-}G/G}$;*WAP-Tgfa* and *Fgfr4*$^{rs351855\text{-}A/A}$;*WAP-Tgfa*) and lung (27) (*Fgfr4*$^{rs351855\text{-}G/G}$;*SPC-CrafBxB* and *Fgfr4*$^{rs351855\text{-}A/A}$;*SPC-CrafBxB*) cancers revealed a significant increase in the proportions of $CD4^{+}CD25^{+}FOXP3^{+ve}$ regulatory T cells in the tumors extracted from *Fgfr4*$^{rs351855\text{-}A/A}$ knock-in mice (Figure 4A, B). Furthermore, the significant increase in tumor-infiltrating $T_{REGs}$ correlated with increased $T_{REGs}$ in lymphoid organs (data not shown) and elevated serum levels of IL10 in *Fgfr4*$^{rs351855\text{-}A/A}$;*WAP-Tgfa* (Figure 4C) and *Fgfr4*$^{rs351855\text{-}A/A}$;*SPC-CrafBxB* (Figure 4D) mice. On the other hand, a marked reduction in the numbers of tumor-infiltrating $CD8^{+ve}$ T cells was observed in the *Fgfr4*$^{rs351855\text{-}A/A}$ cohorts

of GEKIMMs for both breast (Figure 4E) and lung (Figure 4F) cancers. Although STAT3 signaling is considered crucial for T helper cell differentiation during immune challenges, in both transgenic disease models for cancers, we did not observe any significant differences between the two genotypes. The proportions of differentiated $CD4^{+ve}$ T cell subsets, namely, Th1, Th2 and Th17, in spleens and tumors of GEKIMM for lung cancer (Supplemental Figure 10) and the GEKIMM for breast cancer (Supplemental Figure 11), were not altered. We propose that the differences in these subsets may be notable in the mouse models for inflammation-induced cancers. Collectively, through data from knock-in mice, knockout mice and genetically engineered knock-in mouse models for lung and breast cancers, our study unequivocally illustrates a pleiotropic effect of cancer-associated STAT3-enhancing germline variants in shaping some aspects of the tumor microenvironment (Supplemental Figure 12). Hence, we conclude that the immune evasive phenotype of the tumor microenvironment can be determined by the pleiotropic functions of individual-specific germline variants in the immune cells. In this regard, cancer-associated germline receptor variants that enhance the amplitude of STAT3 signaling are potent modulators of tumor-intrinsic proliferative and tumor-extrinsic immune evasive functions. Overall, our work provides valuable insights into the prognostic value of STAT3 enhancing germline receptor variants in the immune-excluded and immunologically ignorant tumor phenotype. Given that the germline encoded STAT3-enhancing SNPs are particularly prevalent in the coding regions of immune cell surface markers, further work is warranted to explore their significance as predictive biomarkers for immunotherapy responses.

## Methods

A complete description of the methods and statistical analysis is provided in the Supplemental Materials

## Author Contributions

VKU conceived and designed this study. DK wrote the codes for TraPS-VarI algorithm. VKU and DK performed the computation analyses. AG, CY and CF performed the immune phenotyping analyses for the *Fgfr4* knock-out mice. VKU performed the experiments, analysed the data, interpreted the results, and wrote the manuscript. The final version of the manuscript was reviewed by all the co-authors.

## Acknowledgements

The authors thank Prof. Axel Ullrich for reading the drafts of this manuscript and generously supporting this work, Susanne Wuchenauer and Bianca Sperl for technical assistance. The authors acknowledge Heinz Brandstetter and Corrina Moerth for their services with the animal housing facilities. A.G and C.F are supported in part by the American Heart Association. C.F supported by the American Diabetes Association, and the grant R01HL128714 from the National Institutes of Health supported part of the work.

## Disclosures

C.F. has served as a consultant or received honoraria from Ultragenyx and has received research support from U3 Pharma GmbH and Roche.

# References


1. Hanahan, D., and Weinberg, R.A. 2011. Hallmarks of Cancer: The Next Generation. *Cell* 144:646-674.
2. Hoos, A. 2016. Development of immuno-oncology drugs [mdash] from CTLA4 to PD1 to the next generations. *Nat Rev Drug Discov* 15:235-247.
3. Palucka, A.K., and Coussens, L.M. The Basis of Oncoimmunology. *Cell* 164:1233-1247.
4. Fridman, W.H., Pages, F., Sautes-Fridman, C., and Galon, J. 2012. The immune contexture in human tumours: impact on clinical outcome. *Nat Rev Cancer* 12:298-306.
5. Kroemer, G., Galluzzi, L., Kepp, O., and Zitvogel, L. 2013. Immunogenic Cell Death in Cancer Therapy. *Annual Review of Immunology* 31:51-72.
6. Dunn, G.P., Old, L.J., and Schreiber, R.D. 2004. The Three Es of Cancer Immunoediting. *Annual Review of Immunology* 22:329-360.
7. Ulaganathan, V.K., and Ullrich, A. 2016. Membrane-proximal binding of STAT3 revealed by cancer-associated receptor variants. *Molecular & Cellular Oncology* 3:e1145176.
8. Wang, T., Niu, G., Kortylewski, M., Burdelya, L., Shain, K., Zhang, S., Bhattacharya, R., Gabrilovich, D., Heller, R., Coppola, D., et al. 2004. Regulation of the innate and adaptive immune responses by Stat-3 signaling in tumor cells. *Nat Med* 10:48-54.
9. Cheng, F., Wang, H.-W., Cuenca, A., Huang, M., Ghansah, T., Brayer, J., Kerr, W.G., Takeda, K., Akira, S., Schoenberger, S.P., et al. 2003. A Critical Role for Stat3 Signaling in Immune Tolerance. *Immunity* 19:425-436.
10. Sun, Z., Yao, Z., Liu, S., Tang, H., and Yan, X. 2006. An oligonucleotide decoy for Stat3 activates the immune response of macrophages to breast cancer. *Immunobiology* 211:199-209.
11. Yu, H., Kortylewski, M., and Pardoll, D. 2007. Crosstalk between cancer and immune cells: role of STAT3 in the tumour microenvironment. *Nat Rev Immunol* 7:41-51.
12. The Genomes Project, C. 2015. A global reference for human genetic variation. *Nature* 526:68-74.
13. Forbes, S.A., Beare, D., Gunasekaran, P., Leung, K., Bindal, N., Boutselakis, H., Ding, M., Bamford, S., Cole, C., Ward, S., et al. 2015. COSMIC: exploring the world's knowledge of somatic mutations in human cancer. *Nucleic Acids Research* 43:D805-D811.
14. Barretina, J., Caponigro, G., Stransky, N., Venkatesan, K., Margolin, A.A., Kim, S., Wilson, C.J., Lehar, J., Kryukov, G.V., Sonkin, D., et al. 2012. The Cancer Cell Line Encyclopedia enables predictive modelling of anticancer drug sensitivity. *Nature* 483:603-307.
15. Sherry, S.T., Ward, M.H., Kholodov, M., Baker, J., Phan, L., Smigielski, E.M., and Sirotkin, K. 2001. dbSNP: the NCBI database of genetic variation. *Nucleic Acids Research* 29:308-311.
16. Lek, M., Karczewski, K.J., Minikel, E.V., Samocha, K.E., Banks, E., Fennell, T., O,ÄôDonnell-Luria, A.H., Ware, J.S., Hill, A.J., Cummings, B.B., et al. 2016. Analysis of protein-coding genetic variation in 60,706 humans. *Nature* 536:285-291.
17. 2003. The International HapMap Project. *Nature* 426:789-796.
18. Reinhold, W.C., Varma, S., Sousa, F., Sunshine, M., Abaan, O.D., Davis, S.R., Reinhold, S.W., Kohn, K.W., Morris, J., Meltzer, P.S., et al. 2014. NCI-60 Whole Exome Sequencing and Pharmacological CellMiner Analyses. *PLOS ONE* 9:e101670.
19. The Cancer Genome Atlas Research, N., Weinstein, J.N., Collisson, E.A., Mills, G.B., Shaw, K.R.M., Ozenberger, B.A., Ellrott, K., Shmulevich, I., Sander, C., and Stuart, J.M. 2013. The Cancer Genome Atlas Pan-Cancer analysis project. *Nat Genet* 45:1113-1120.
20. Erikson, G.A., Bodian, D.L., Rueda, M., Molparia, B., Scott, E.R., Scott-VanZeeland, A.A., Topol, S.E., Wineinger, N.E., Niederhuber, J.E., Topol, E.J., et al. 2016. Whole-Genome Sequencing of a Healthy Aging Cohort. *Cell* 165:1002-1011.
21. Kogan, D., and Ulaganathan, V.K. 2017. TraPS-VarI: a python module for the identification of STAT3 modulating germline receptor variants. *bioRxiv*.
22. Kuczma, M., Podolsky, R., Garge, N., Daniely, D., Pacholczyk, R., Ignatowicz, L., and Kraj, P. 2009. Foxp3-Deficient Regulatory T Cells Do Not Revert into Conventional Effector CD4+ T Cells but Constitute a Unique Cell Subset. *The Journal of Immunology* 183:3731-3741.
23. Weber-Nordt, R.M., Riley, J.K., Greenlund, A.C., Moore, K.W., Darnell, J.E., and Schreiber, R.D. 1996. Stat3 Recruitment by Two Distinct Ligand-induced, Tyrosine-phosphorylated Docking Sites in the Interleukin-10 Receptor Intracellular Domain. *Journal of Biological Chemistry* 271:27954-27961.
24. Ulaganathan, V.K., Sperl, B., Rapp, U.R., and Ullrich, A. 2015. Germline variant FGFR4 p.G388R exposes a membrane-proximal STAT3 binding site. *Nature* 528:570-574.
25. Seitzer, N., Mayr, T., Streit, S., and Ullrich, A. 2010. A Single Nucleotide Change in the Mouse Genome Accelerates Breast Cancer Progression. *Cancer Research* 70:802-812.
26. Sandgren, E.P., Schroeder, J.A., Qui, T.H., Palmiter, R.D., Brinster, R.L., and Lee, D.C. 1995. Inhibition of Mammary Gland Involution Is Associated with Transforming Growth Factor α but not c-myc-induced Tumorigenesis in Transgenic Mice. *Cancer Research* 55:3915-3927.

27. Kerkhoff, E., Fedorov, L.M., Siefken, R., Walter, A.O., Papadopoulos, T., and Rapp, U.R. 2000. Lung-targeted Expression of the c-Raf-1 Kinase in Transgenic Mice Exposes a Novel Oncogenic Character of the Wild-Type Protein. *Cell Growth Differ* 11:185-190.

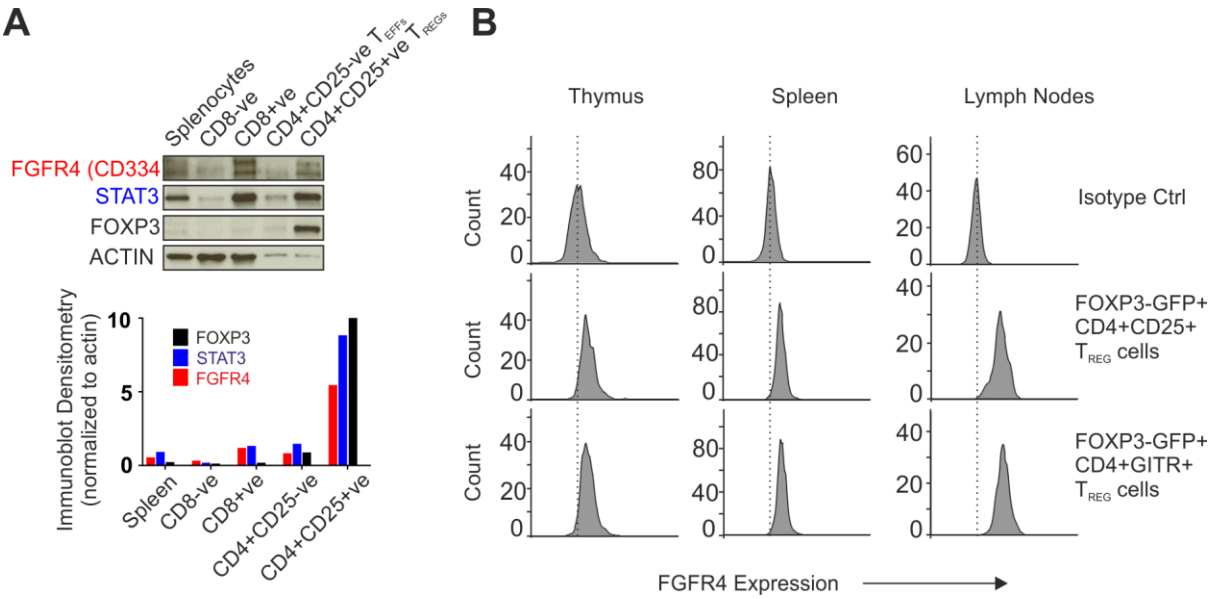


**Figure 1. Expression analysis of FGFR4 in lymphocytes.**

(**A**) Representative immunoblot analysis of FGFR4, STAT3 and FOXP3 proteins in purified and pooled lymphocytes (n=13 adult mice). The histogram below shows digital quantification normalized to actin expression bands. The data shown are representative of 3 independent cell isolation and immunoblot experiments.

(**B**) Expression analysis for FGFR4 in CD4+CD25+ and CD4+GITR+ regulatory lymphocytes using fluorochrome-conjugated antibodies in blood, mesenteric lymph nodes, spleens and thymuses isolated from 7-month-old *Foxp3-GFP* reporter mice. Plots are representative of 5 independent biological replicates.

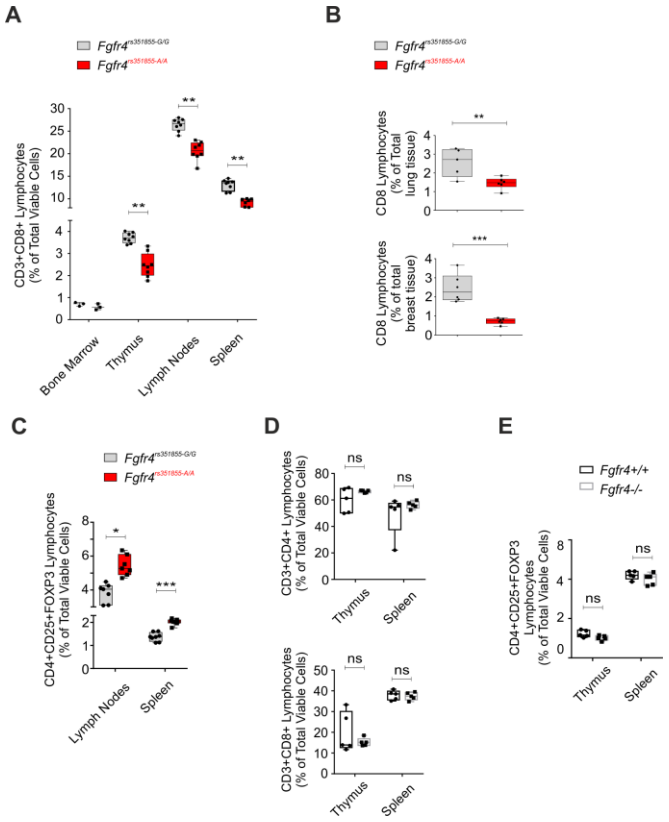


**Figure 2. Rs351855 SNP-specific suppression of the CD8:$T_{REG}$ ratio in healthy tissues.**

(**A**) Analysis of $CD8^{+ve}$ T cells in bone marrow, thymus, blood, lymph nodes and spleens of 6- to 8-week-old *Fgfr4*$^{rs351855\text{-}A/A}$ and *Fgfr4*$^{rs351855\text{-}G/G}$ mice quantified by flow cytometry. Data represent the percentages of the total single cell suspension (mean ± S.E.M, n = 5-8, *p < 0.05, **p < 0.01, Statistical comparisons of groups were performed using 2-way ANOVA, Tukey's multiple comparisons test).

(**B**) Analysis of the $CD8^{+ve}$ T cell content in the non-lymphoid parenchymal organs, namely, lung (5 months old) (mean ± S.E.M, n = 6-8, **p < 0.01) and breast tissue (3 months after pregnancy) (mean ± S.E.M, n = 3-4, ***p < 0.001), in *Fgfr4*$^{rs351855\text{-}A/A}$ and *Fgfr4*$^{rs351855\text{-}G/G}$ mice. Infiltrating cells were measured by preparing single cell suspensions.

(**C**) Analysis of $CD4^{+}CD25^{+}FOXP3^{+ve}$ T cell numbers by flow cytometry of live splenocytes from *Fgfr4*$^{rs351855\text{-}A/A}$ and *Fgfr4*$^{rs351855\text{-}G/G}$ mice. Data represent the percentages of total single cell suspensions (mean ± S.E.M, n = 5-8, *p < 0.05, ***p < 0.001, Statistical comparisons of groups was performed by using 2-way ANOVA, Tukey's multiple comparisons test).

(**D**) Quantitative analysis of CD4+ve and CD8+ve cells in the thymus and spleen of 6- to 8-week-old *Fgfr4+/+* and *Fgfr4-/-* mice and **(E)** CD4+CD25+FOXP3+ cells in the thymus and spleen of 6- to 8-week-old *Fgfr4+/+* and *Fgfr4-/-* mice measured by flow cytometry. Data represent the percentages of total single cell suspensions (mean ± S.E.M, n = 5-6, *p < 0.05, ***p < 0.001, Statistical comparisons of groups was performed by using 2-way ANOVA, Tukey's multiple comparisons test). All flow cytometry measurements on wild-type and mutant cohorts of mice were performed on the same day.

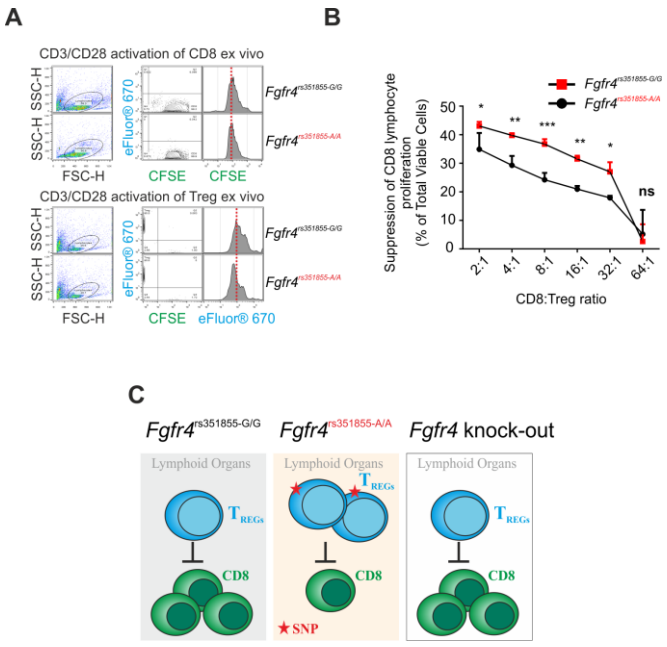


**Figure 3. Genotype-specific suppression of the CD8:$T_{REG}$ ex vivo.**

(**A**) Dye dilution assay assessing the proliferative capacities of eFluor670 and CFSE loaded $CD4^{+}CD25^{+ve}$ $T_{REGs}$ and CD8 T cells, respectively, 72 hours after CD3/CD28 stimulation of isolated from spleens of *Fgfr4*$^{rs351855\text{-}A/A}$ and *Fgfr4*$^{rs351855\text{-}G/G}$ mice.

(**B**) In vitro suppression assays with CD4+CD25+ $T_{REGs}$ from *Fgfr4*$^{rs351855\text{-}G/G}$ and *Fgfr4*$^{rs351855\text{-}A/A}$ mice together with CD8 T cells from *Fgfr4*$^{rs351855\text{-}G/G}$ and *Fgfr4*$^{rs351855\text{-}A/A}$ mice, respectively. $T_{REGs}$ and CD8 T cells were mixed at different ratios and stimulated using mouse T-activator CD3/CD28 Dynabeads. Three days post-stimulation, the percentage of suppression was calculated as described in the Methods section. Data are representative of three independent experiments. For each experiment, cells were isolated from a group of 5 mice of either genotype, and each mixed ratio was co-cultivated in replicates of 5 wells (mean ± S.E.M; ns = not significant; *p < 0.05, **p < 0.01, ***p < 0.001, two-way ANOVA using Sidak's multiple comparisons test).

(**C**) Graphical summary illustrating the SNP-specific gain of immunological function by the minor allele (NC_000005.10:g.177093242G>A) of the rs351855 SNP. The genotype-dependent phenotype is abolished in the FGFR4-deficient mice and indistinguishable from the wild-type FGFR4 variant expressing cohorts indicative of enhanced rs351855 G>A-variant-specific STAT3 signaling in lymphoid organs.

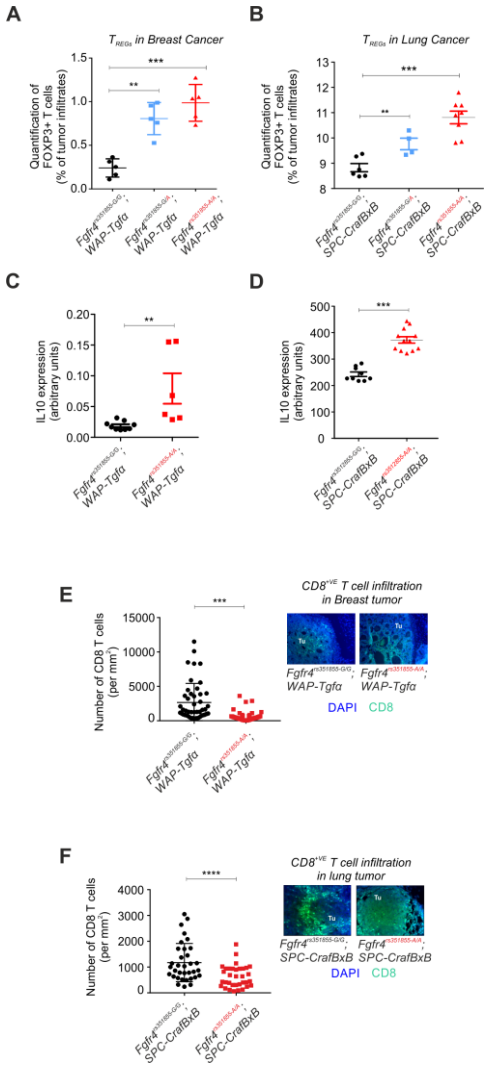


**Figure 4. Rs351855 SNP-specific suppression of the CD8:T$_{REG}$ in the tumor microenvironment.**

(**A**) Numbers of CD4$^{+}$CD25$^{+}$FOXP3$^{+ve}$ T cells in tumor-bearing breast tissues of *Fgfr4$^{rs351855\text{-}G/G}$;Wap-Tgfa*, *Fgfr4$^{rs351855\text{-}G/A}$;Wap-Tgfa* and *Fgfr4$^{rs351855\text{-}A/A}$;Wap-Tgfa* mice (mean ± S.E.M, n = 5, *p < 0.05) and (**B**) tumor-bearing lungs of *Fgfr4$^{rs351855\text{-}G/G}$; SPC-CrafBxB, Fgfr4$^{rs351855\text{-}G/A}$; SPC-CrafBxB* and *Fgfr4$^{rs351855\text{-}A/A}$;SPC-CrafBxB* mice (mean ± S.E.M, n = 4-7, **p < 0.01, ***p < 0.001).

(**C**) Quantification of IL10 in serums of tumor-bearing *Fgfr4$^{rs351855\text{-}G/G}$;Wap-Tgfa* and *Fgfr4$^{rs351855\text{-}A/A}$;Wap-Tgfa* breast cancer mice (mean ± S.E.M, n = 6-9, **p < 0.01) and tumor-bearing *Fgfr4$^{rs351855\text{-}G/G}$; SPC-CrafBxB* and *Fgfr4$^{rs351855\text{-}A/A}$;SPC-CrafBxB* lung cancer mice (mean ± S.E.M, n = 8-12, ***p < 0.001) by ELISA.

(**E, F**) Quantification of tumor-infiltrating CD8$^{+ve}$ T cells in tumor nodules by immune staining for CD8 in breast tumor-bearing *Fgfr4$^{rs351855\text{-}G/G}$;Wap-Tgfa* and *Fgfr4$^{rs351855\text{-}A/A}$;Wap-Tgfa* mice and (**F**) lung tumor-bearing *Fgfr4$^{rs351855\text{-}G/G}$; SPC-CrafBxB* and *Fgfr4$^{rs351855\text{-}A/A}$;SPC-CrafBxB* (mean ± SEM, n = 19-26, ****p < 0.0001, ***p < 0.001, ns = not significant two-tailed unpaired t-test with Welch's correction). (**Inset images**) Representative images from immunofluorescence staining of tumor sections (20X magnification) depicting tumor-infiltrating CD8+ T cells in lung and breast tumors (DAPI-blue; CD8-green).

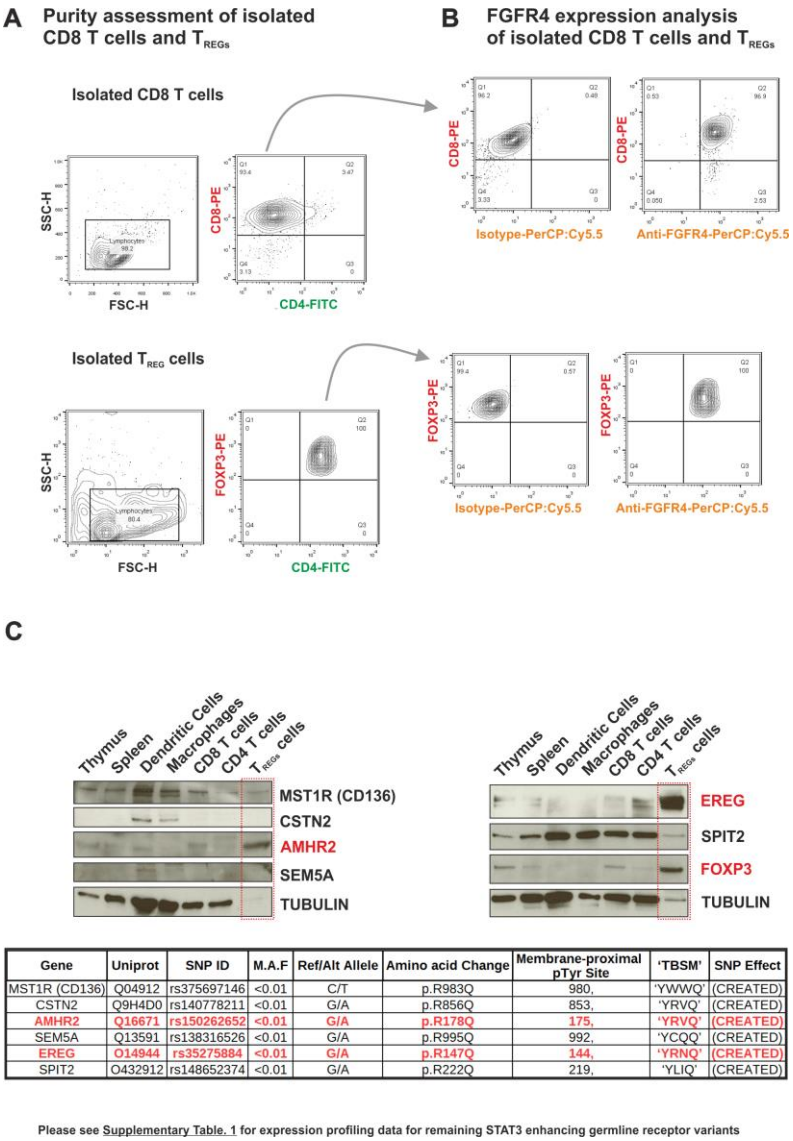


| Gene | Uniprot | SNP ID | M.A.F | Ref/Alt Allele | Amino acid Change | Membrane-proximal pTyr Site | 'TBSM' | SNP Effect |
|---|---|---|---|---|---|---|---|---|
| MST1R (CD136) | Q04912 | rs375697146 | <0.01 | C/T | p.R983Q | 980, | 'YWWQ' | (CREATED) |
| CSTN2 | Q9H4D0 | rs140778211 | <0.01 | G/A | p.R856Q | 853, | 'YRVQ' | (CREATED) |
| AMHR2 | Q16671 | rs150262652 | <0.01 | G/A | p.R178Q | 175, | 'YRVQ' | (CREATED) |
| SEM5A | Q13591 | rs138316526 | <0.01 | G/A | p.R995Q | 992, | 'YCQQ' | (CREATED) |
| EREG | O14944 | rs35275884 | <0.01 | G/A | p.R147Q | 144, | 'YRNQ' | (CREATED) |
| SPIT2 | O432912 | rs148652374 | <0.01 | G/A | p.R222Q | 219, | 'YLIQ' | (CREATED) |

Please see Supplementary Table. 1 for expression profiling data for remaining STAT3 enhancing germline receptor variants

**Supplemental Figure 1. Expression analysis of STAT3 enhancing germline variants in purified CD8+ and CD4+CD25+ cells.**

(**A**) Representative flow cytometry expression analysis (left) and (**B**) quantification (right) of phosphorylated STAT3 [pSTAT3 (Y705)] assessed by gating on $CD4^{+}FOXP3^{+ve}$ T cells in total splenocytes derived from *Fgfr4*$^{rs351855G/G}$ (homozygous) (n=5), *Fgfr4*$^{rs351855-G/A}$ (heterozygous) (n=4) and *Fgfr4*$^{rs351855-A/A}$ (homozygous) (n=5) mice. MFI, mean fluorescence intensity. Histogram shows mean fluorescence intensity (mean ± S.E.M, *p < 0.05, two-tailed Student's *t* test).

(**C**) Purity assessment of isolated $CD8^{+ve}$ T cells and $CD4^{+}CD25^{+ve}$ $T_{REGs}$ from spleens of 8-month old healthy wild-type mice. Pooled cells isolated from several (n= 13) C57bl/6 age-matched mice were evaluated for expression of (**D**) FGFR4 by FACS staining for CD4, CD8, CD25, FOXP3 markers and (**E**) MST1R, CSTN2, AMHR2, SEMA5A, EREG, SPIT2 by immunoblot analyses. Expression analyses of all remaining human germline variants containing a membrane-proximal STAT3 recruiting motif is shown in the Supplementary Table 1.

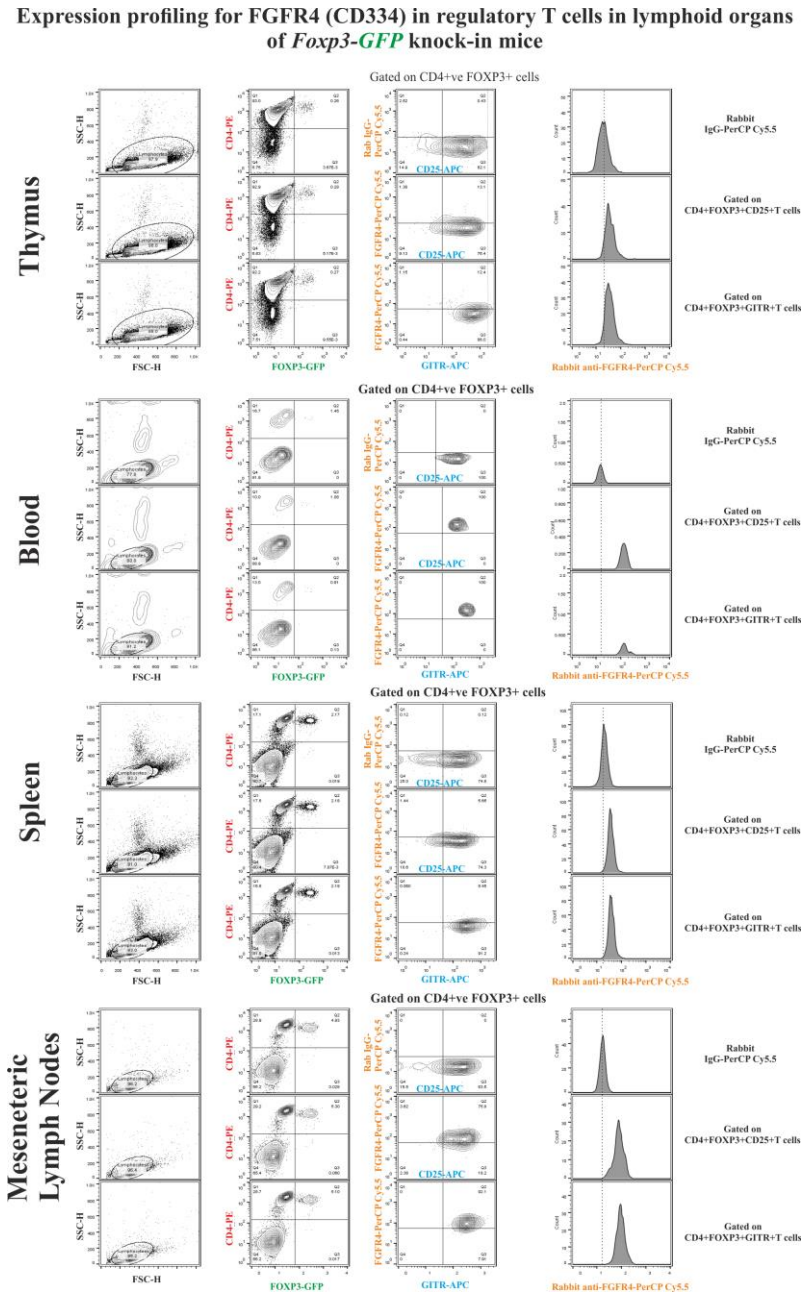


**Supplemental Figure 2. Expression analysis for FGFR4 in $T_{REGs}$ using *Foxp3-GFP* knock-in reporter mice.**

Shown are representative images of results from flow cytometry based surface staining for CD4, CD25 and GITR markers and intracellular staining for FGFR4 using directly labeled antibodies. $CD4^{+}CD25^{+}FOXP3^{+}GFP^{+ve}$ $T_{REGs}$ and $CD4^{+}GITR^{+}FOXP3^{+}GFP^{+ve}$ $T_{REGs}$ in blood, mesenteric lymph nodes, spleens and thymus isolated from 7-month old Foxp3-GFP reporter mice were stained for FGFR4 expression using directly PerCP-Cy5.5 labeled rabbit anti-FGFR4 antibody.

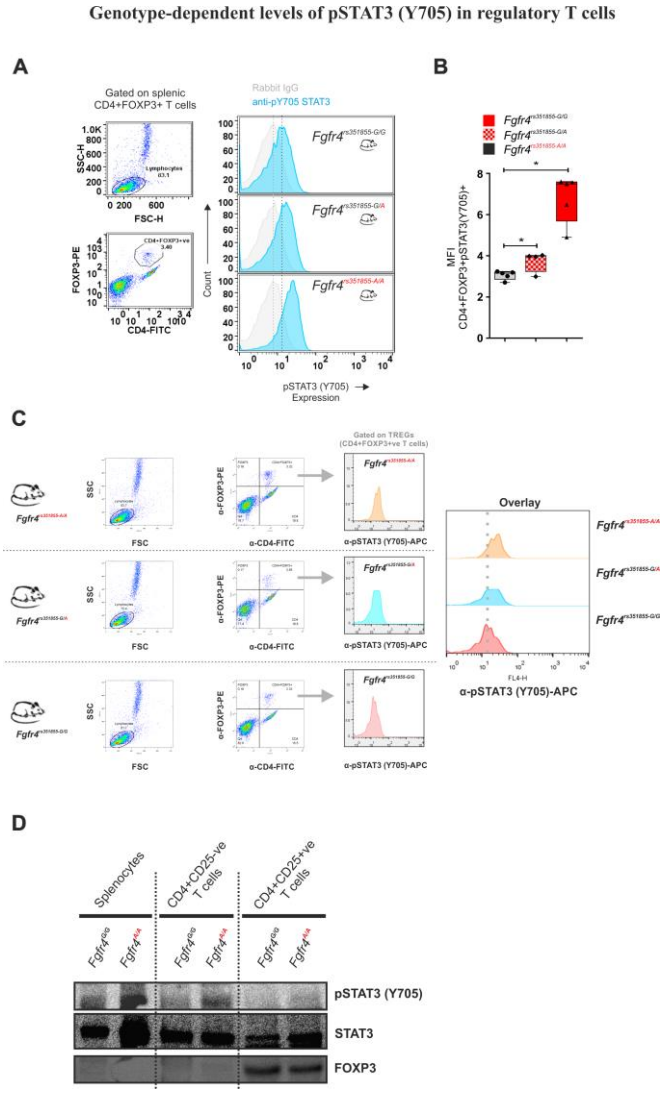


**Supplemental Figure 3. Expression analysis for phosphorylated STAT3 (Y705) in CD4$^{+}$FOXP3$^{+ve}$ regulatory T cells in rs351855-A knock-in mice.**

(**A**) Representative flow cytometry expression analysis (left) and (**B**) quantification (right) of phosphorylated STAT3 [pSTAT3 (Y705)] assessed by gating on CD4$^{+}$FOXP3$^{+ve}$ T cells in total splenocytes derived from *Fgfr4*$^{rs351855G/G}$ (homozygous) (n=5), *Fgfr4*$^{rs351855-G/A}$ (heterozygous) (n=4) and *Fgfr4*$^{rs351855-A/A}$ (homozygous) (n=5) mice. MFI, mean fluorescence intensity. Histogram shows mean fluorescence intensity (mean ± S.E.M, *p < 0.05, two-tailed Student's *t* test).

(**C**) Triple staining for CD4, FOXP3 and pSTAT3 (Y705) in total splenocytes of *Fgfr4*$^{rs351855G/G}$ (homozygous), *Fgfr4*$^{rs351855-G/A}$ (heterozygous) and *Fgfr4*$^{rs351855-A/A}$ (homozygous) mice. Expression levels of phosphorylated STAT3 (Y705) was assessed by gating on CD4$^{+}$FOXP3$^{+ve}$ $T_{REGs}$.

(**D**) Immunoblot detection of pSTAT3 (Y705), STAT3 and FOXP3 protein levels in purified CD4+CD25-ve and CD4+CD25+ T cells isolated from *Fgfr4*$^{rs351855G/G}$ and *Fgfr4*$^{rs351855-A/A}$ transgenic mice (splenocytes pooled from n=5 mice)

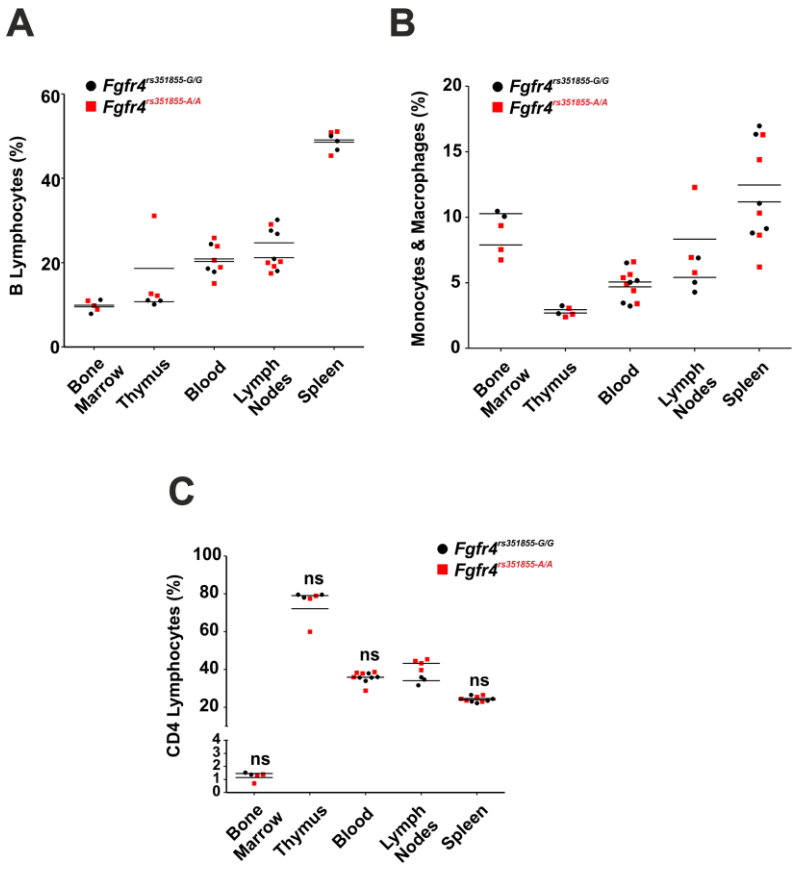


**Supplemental Figure 4. Quantification of B cells, monocytes and CD4 T cells in healthy SNP knock-in transgenic mice.**

(**A**) Flow cytometry analyses of CD19$^{+ve}$ B cells in bone marrow, thymus, blood, lymph nodes and spleen extracted from *Fgfr4*$^{rs351855G/G}$ and *Fgfr4*$^{rs351855-A/A}$ homozygous mice at 6-8 weeks of age. Date represent percentage of cells (mean ± S.E.M, n = 3-5 mice per group, **p < 0.01, ns = not significant)

(**B**) Flow cytometry analysis of F4/80 positive monocyte/macrophage cells in bone marrow, thymus, blood, lymph nodes and spleen extracted from *Fgfr4*$^{rs351855G/G}$ and *Fgfr4*$^{rs351855-A/A}$ homozygous mice of 6-8 weeks age. Data represent percentage of cells (mean ± S.E.M, n = 3-5 mice per group, ns = not significant)

(**C**) Flow cytometry analysis of CD4$^{+ve}$ T cells in bone marrow, thymus, blood, lymph nodes and spleen extracted from *Fgfr4*$^{rs351855G/G}$ and *Fgfr4*$^{rs351855-A/A}$ homozygous mice at 6-8 weeks of age. Date represent percentage of cells (mean ± S.E.M, n = 3 to 5 mice per group, ns = not significant)

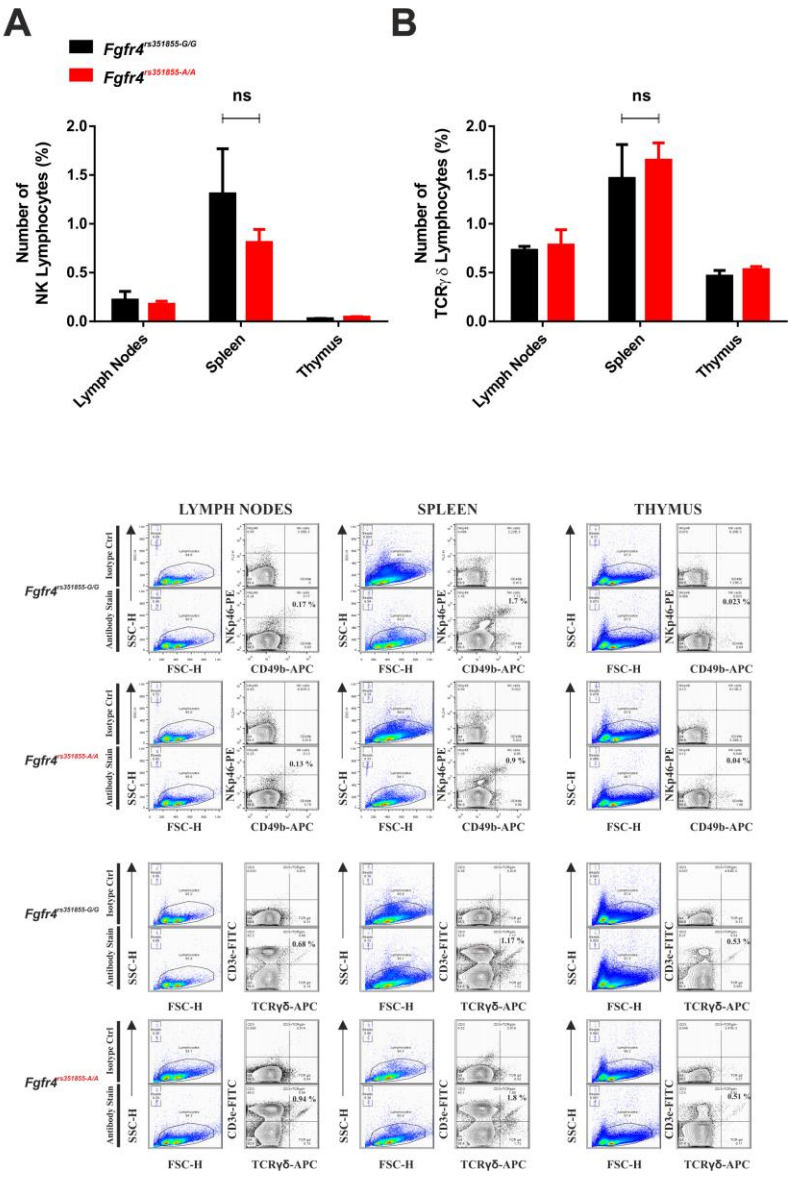


**Supplemental Figure 5. Quantification of NK cells and TCRγδ cell in lymphoid organs of healthy SNP knock-in mice.**

Flow cytometry based enumeration of CD49b and NKp46 double-positive cells and CD3e and TCRγδ double positive cells in mesenteric lymph nodes, spleen and thymus of 8-month old mice of *Fgfr4*$^{rs351855G/G}$ and *Fgfr4*$^{rs351855-A/A}$ genotypes. First two row panels show representative scatter plot and dot blot images of FACS analyses. Bottom row shows histogram analyses of data obtained from 6 mice per group (mean ± S.E.M, n = 6, ns = not significant, two way ANOVA using Sidak's multiple comparisons test).

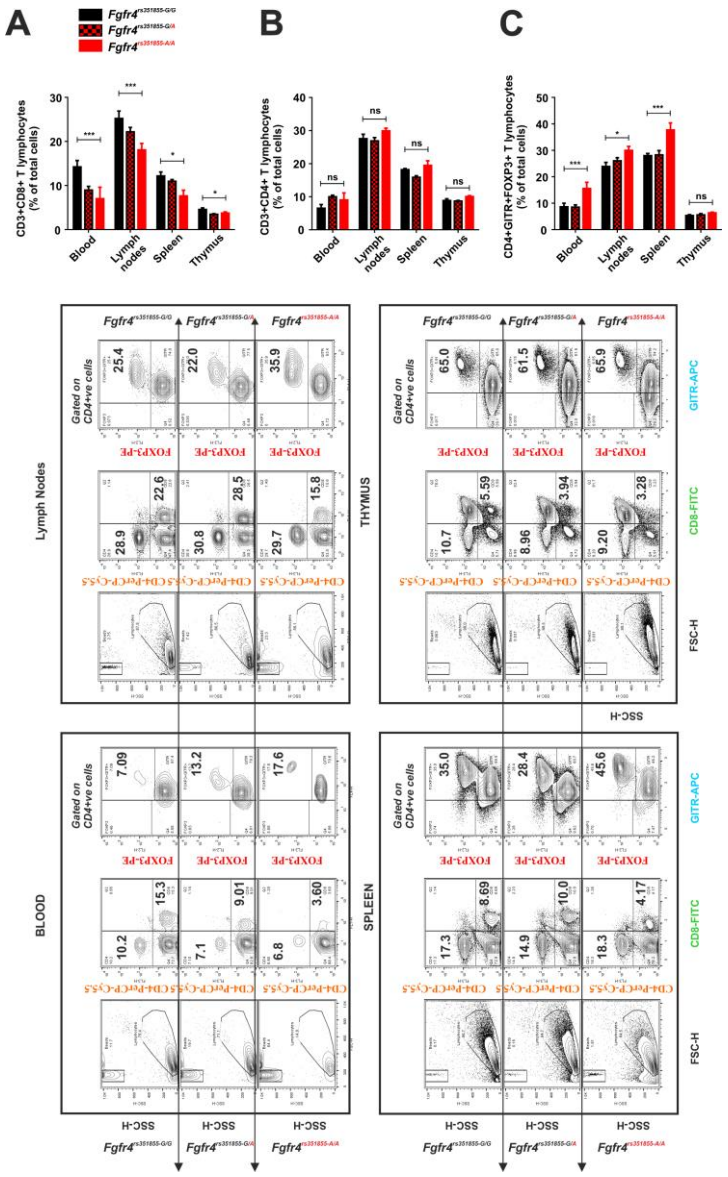


**Supplemental Figure 6. Quantification of CD8, CD4 and $T_{REGs}$ in healthy SNP knock-in mice.**

(**A**) Quantification of $CD8^{+ve}$ and (**B**) $CD4^{+ve}$ T cells by flow cytometry in blood, mesenteric lymph nodes, spleens and thymus isolated from 7-month old mice of the following genotypes: *Fgfr4*$^{rs351855G/G}$, *Fgfr4*$^{rs351855-G/A}$ and *Fgfr4*$^{rs351855-A/A}$.

(**C**) Quantification of regulatory T cells was done by intracellular *staining* for detection of $CD4^{+}GITR^{+}FOXP3^{+ve}$ T cells in blood, mesenteric lymph nodes, spleens and thymus isolated from 7 months mice of following genotypes: *Fgfr4*$^{rs351855G/G}$ , *Fgfr4*$^{rs351855-G/A}$ and *Fgfr4*$^{rs351855-A/A}$. Data shown in (**C**) were analysed by gating on $CD4^{+}GITR^{+ve}$ T cells (mean ± S.E.M; n = 6, ns = not significant; **p < 0.01, ****p < 0.0001; two way ANOVA using Sidak's multiple comparisons test).

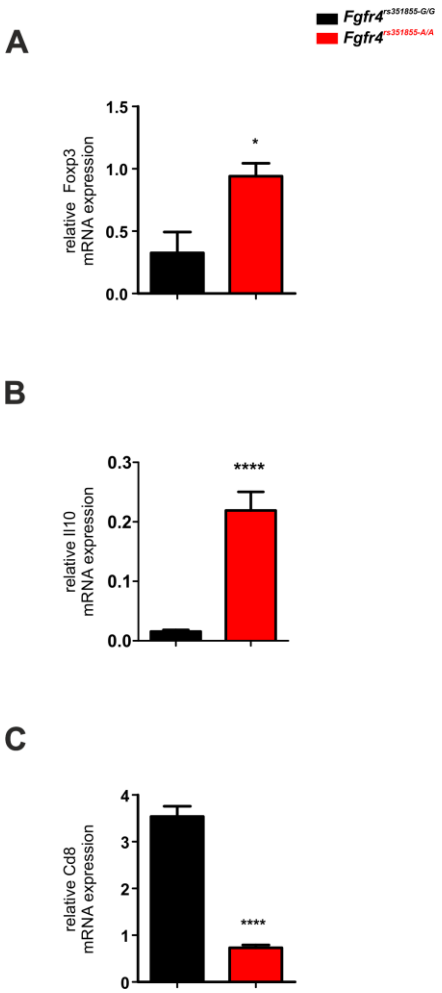


**Supplemental Figure 7. Quantitative real time PCR analysis for CD4, CD8 and IL10.**

Relative abundance of (**A**) *Foxp3*, (**B**) *Il10*, and (**C**) *Cd8* transcripts in spleens of 6-8 week old *Fgfr4*$^{rs351855\text{-}A/A}$ and *Fgfr4*$^{rs351855G/G}$ mice, measured by quantitative real time PCR. Data represent relative mRNA expression normalized to *Hprt* expression (mean ± S.E.M, n = 3, **p < 0.01, ****p < 0.0001, ns = not significant).

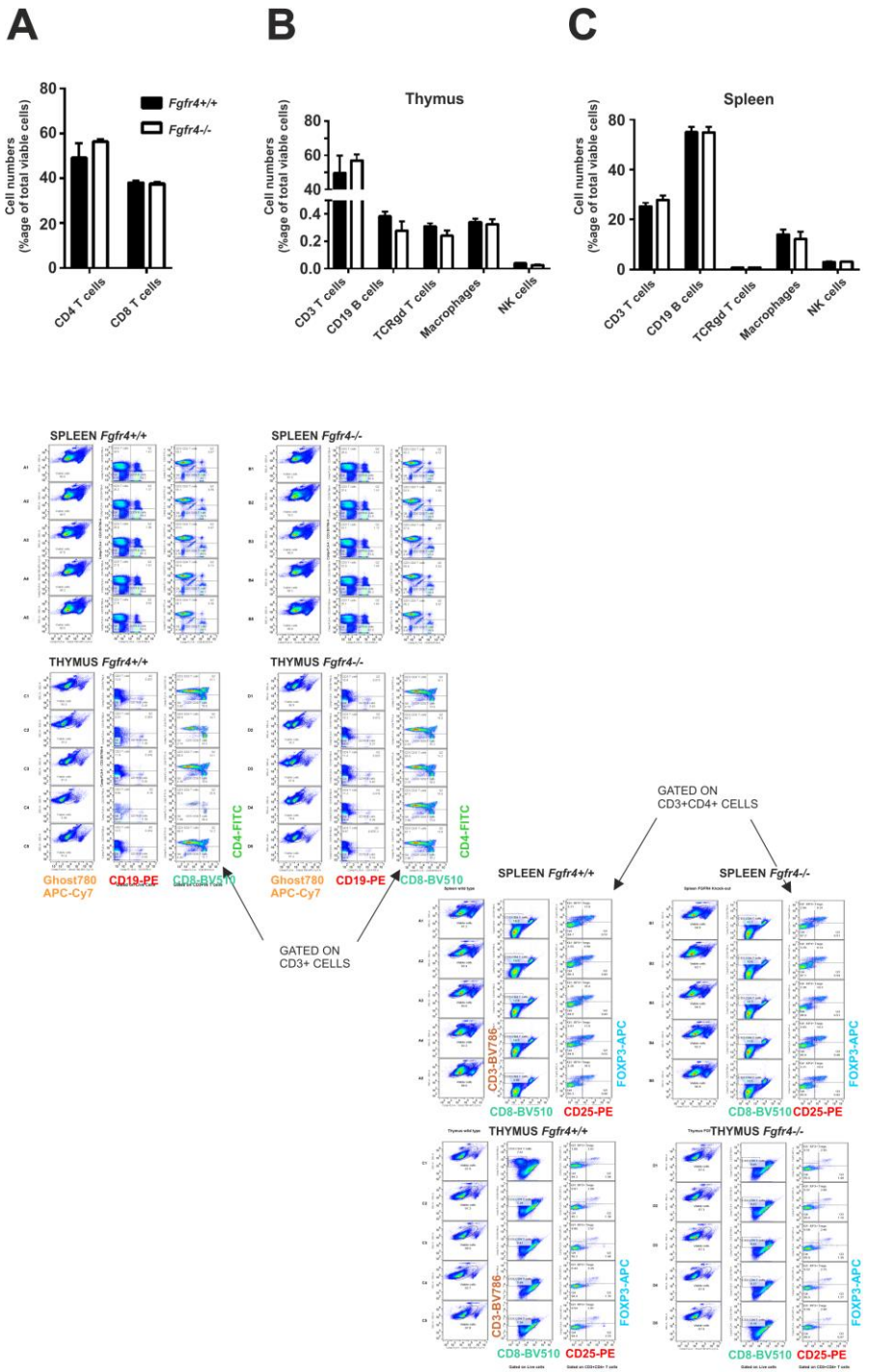


**Supplemental Figure 8. Immunophenotyping analyses of FGFR4 deficient mice.**

(**A**) Quantification of CD4+ and CD8+ T cells in the age- and gender-matched 6-8 week old *Fgfr4* wild-type and knock-out mice is shown. Immune phenotyping analysis by quantitative flow cytometry for T cells, B cells, TCRγδ cells, macrophages and NK cell populations in the (**B**) thymus and (**C**) spleen (mean ± S.E.M, n=5, ns= not significant)..

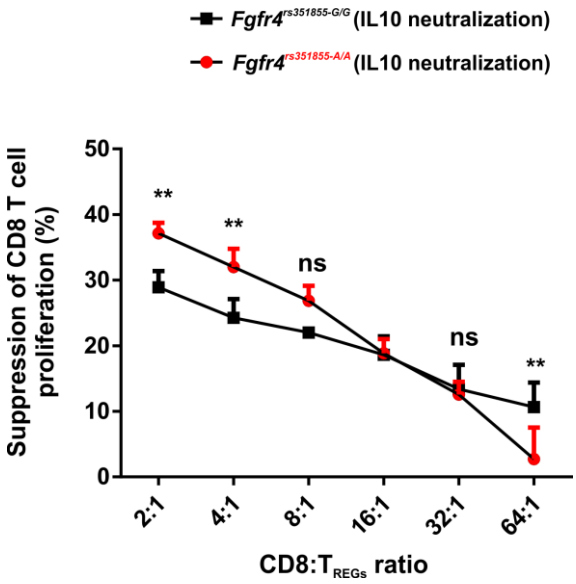


**Supplemental Figure 9. In vitro suppression assay under IL10 neutralization.**

In vitro suppression assays with CD4+CD25+ $T_{REGs}$ from *Fgfr4*$^{rs351855G/G}$ and *Fgfr4*$^{rs351855-A/A}$ mice together with $CD8^{+ve}$ T cells from *Fgfr4*$^{rs351855G/G}$ and *Fgfr4*$^{rs351855-A/A}$ mice, respectively. $T_{REGs}$ and CD8 T cells were mixed at different ratios and stimulated using mouse T-activator CD3/CD28 Dynabeads in the presence of mouse recombinant IL10. Three days post stimulation percentages of suppression were determined as described in the Methods section. Data are representative of at three independent experiments. For each experiments cells were isolated from a group of 5 mice of either genotypes and each mixed ratio co-cultivated in replicates of 5 wells (mean ± S.E.M; ns = not significant; *p < 0.05, **p < 0.01, ***p < 0.001, two way ANOVA using Sidak's multiple comparisons test).

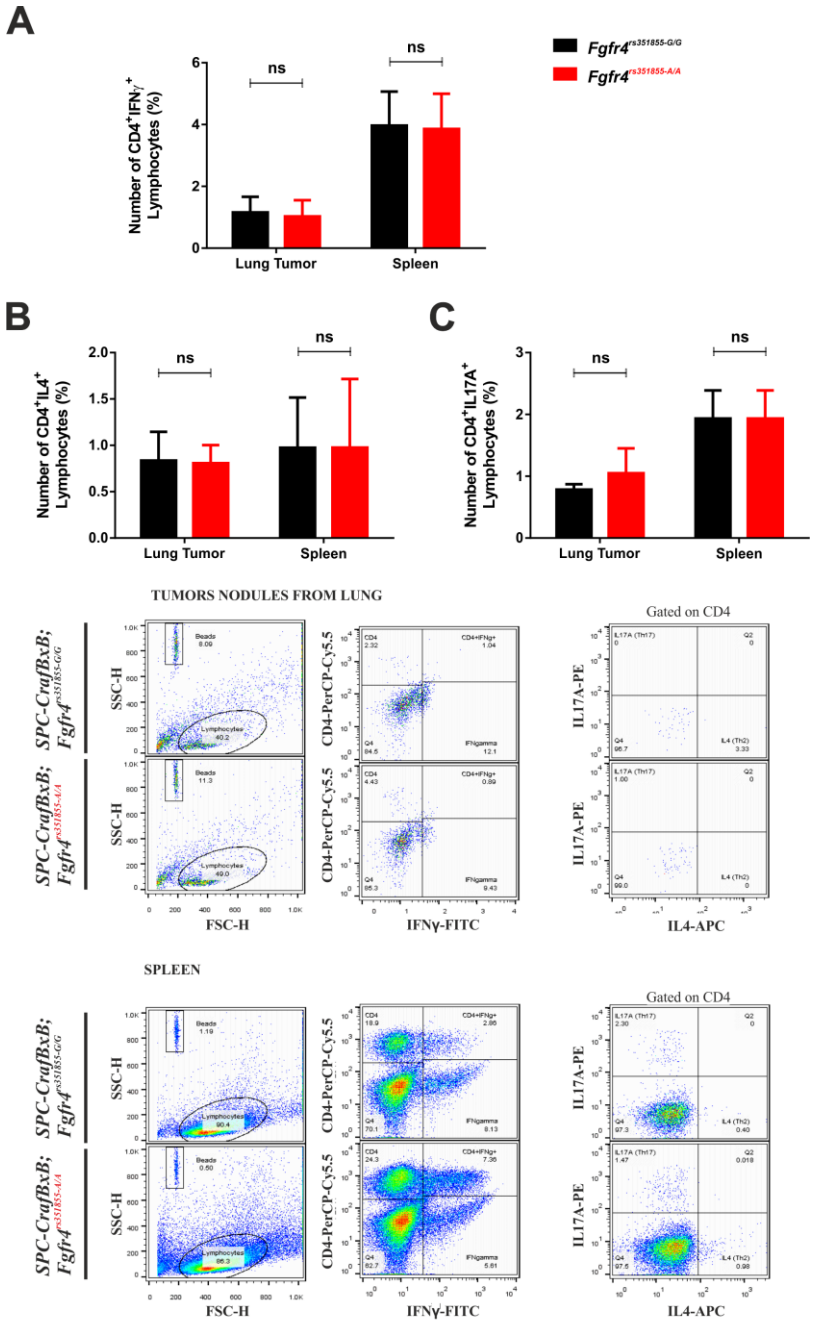


**Supplemental Figure 10. Immunophenotyping analyses for Th1/Th2/Th17 cells in the tumor bearing transgenic mouse model for non-small cell lung cancer.**

Intracellular staining patterns of (**A**) IFNγ, (**B**) IL17A, and (**C**) IL4 in the splenic and tumor infiltrating lymphocytes from 6-month old lung tumor-bearing mice of the following genotypes: *Fgfr4*$^{rs351855G/G}$*;SPC-CrafBxB, Fgfr4*$^{rs351855-G/A}$*;SPC-CrafBxB,* and *Fgfr4*$^{rs351855-A/A}$*;SPC-CrafBxB.* PMA/Ionomycin stimulated spleen cells and tumor infiltrates were stained for CD4, IFNγ, IL17A and IL4. Representative dot blots from five independent experiments for IL17A and IL4 gated on CD4$^{+ve}$ cell populations is shown. Differential numbers of Th1, Th2 and Th17 cells are shown as percentages (mean ± S.E.M, n = 5, ns = not significant, two way ANOVA using Sidak's multiple comparisons test).

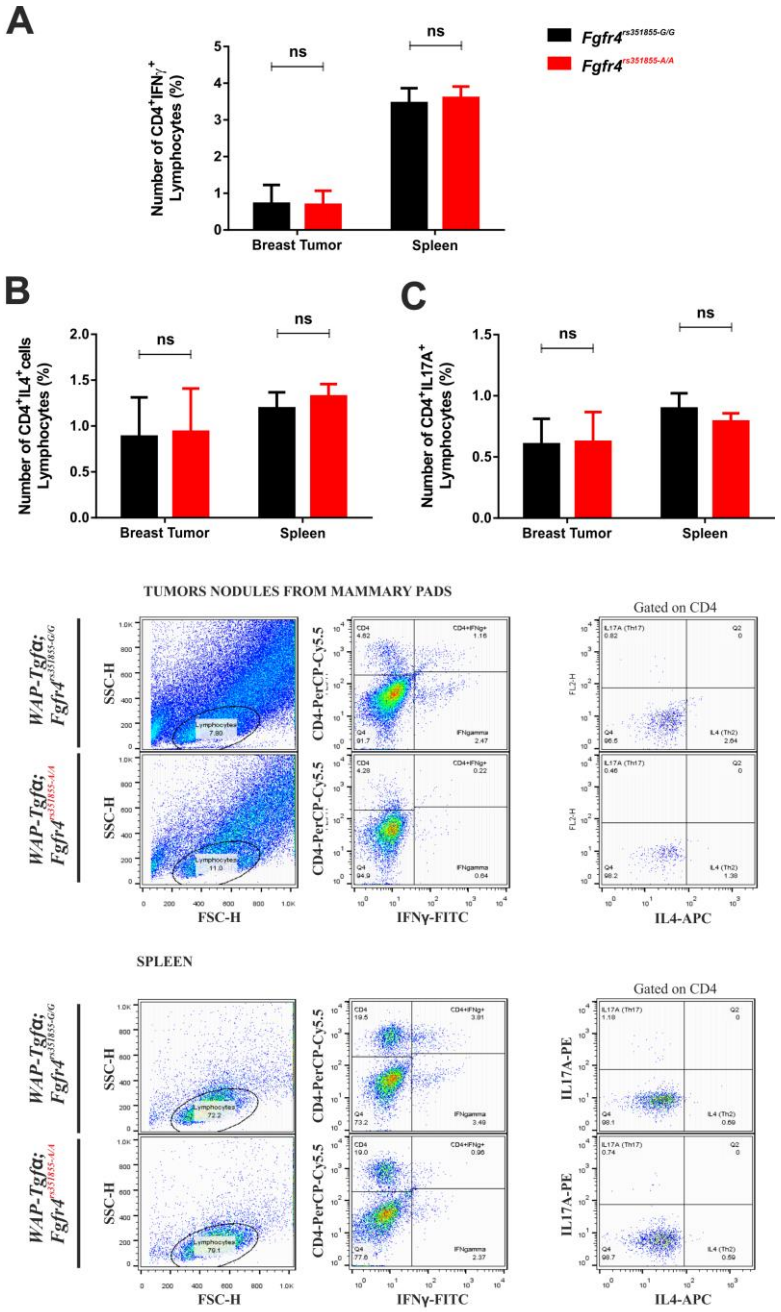


**Supplemental Figure 11. Immunophenotyping analyses for Th1/Th2/Th17 cells in tumor bearing transgenic mouse model for breast cancer.**

Intracellular staining patterns of (**A**) IFNγ, (**B**) IL4, and (**C**) IL17A in the splenic and tumor infiltrating lymphocytes from breast tumor-bearing mice 5 months post-pregnancy of the following genotypes: *Fgfr4*$^{rs351855G/G}$*;WAP-Tgfa, Fgfr4*$^{rs351855-G/A}$*;WAP-Tgfa,* and *Fgfr4*$^{rs351855-A/A}$*; WAP-Tgfa*. PMA/Ionomycin stimulated spleen cells and tumor infiltrates were stained for CD4, IFNγ, IL17A and IL4. Representative dot blots from five independent experiments for IL17A and IL4 gated on CD4+ cell populations is shown. Differential numbers of Th1, Th2 and Th17 cells are shown as percentages (mean ± S.E.M, n = 5, ns = not significant, two way ANOVA using Sidak's multiple comparisons test).

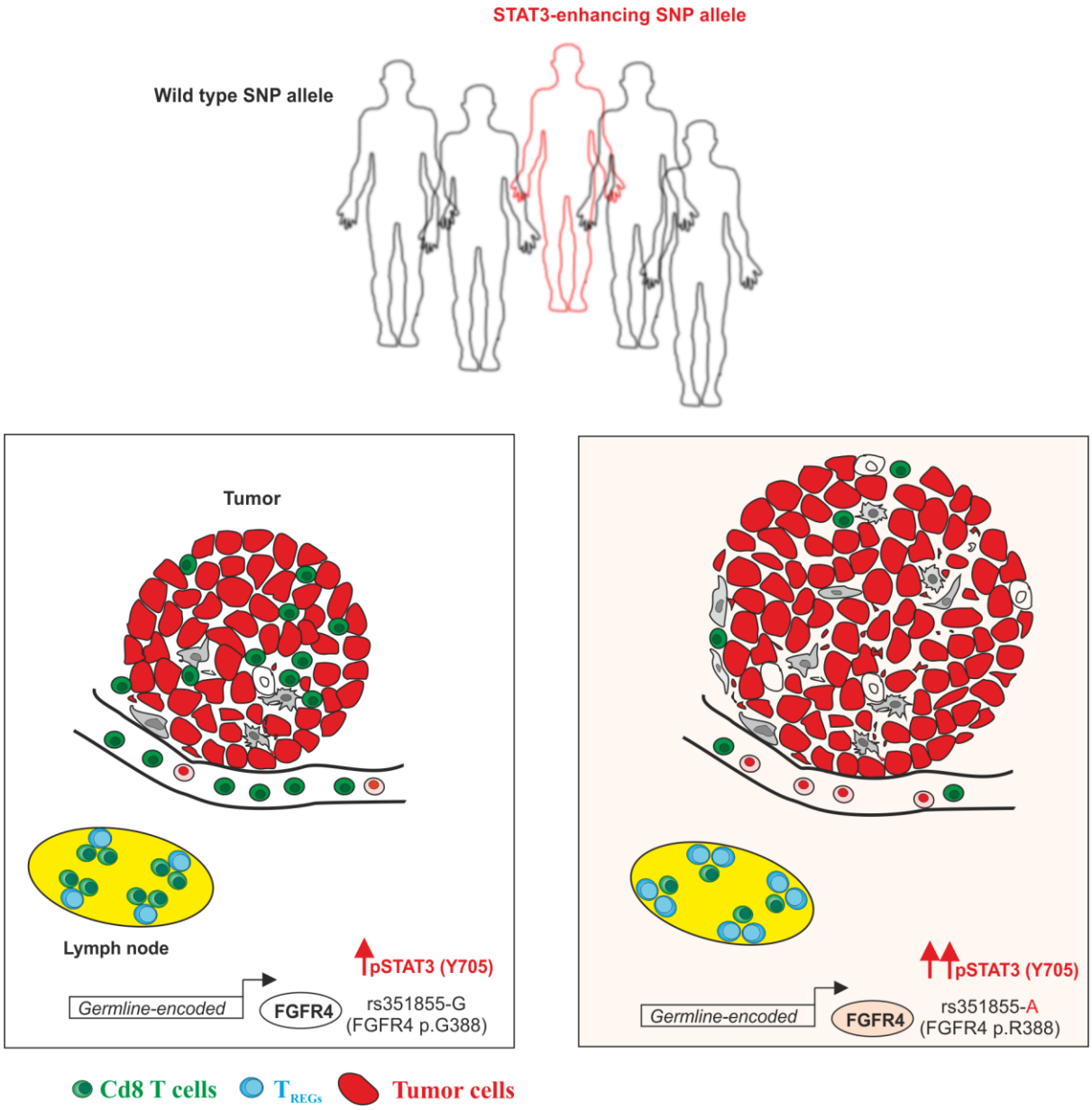


**Supplemental Figure 12. Graphical summary of this study.**

Germline encoded receptor variant such as FGFR4 p.Gly388Arg that enhance the amplitude of STAT3 signaling in regulatory T cells impedes tumor infiltration of $CD8^{+ve}$ T cells by the pleiotropic functions in the immune cells resulting in the general homeostatic suppression of $CD8/T_{REG}$ ratio in vivo.

**Supplemental Table 1.**

Expression analyses by flow cytometry of cell surface receptors in mouse immune cells. Receptors with a germline allele encoding membrane-proximal STAT3 binding sites in humans are listed. MAF = minor allele frequency in the general population. Ref = reference allele and Alt = altered allele.

| S.No | Protein Names | Variation ID | MAF | Ref/ Alt allele | Expression in Immune Subsets | UniProt Accession | Posit-ion | Amino acid change | Mutation type | STAT3 site |
|---|---|---|---|---|---|---|---|---|---|---|
| 1 | NRX1B | rs763582196 | < 0.01 | C/T | CD117+ IL7R- CD150- CD48- AA4.1+ CD43+ HSC BM cells | P58400 | 393 | R->Q | SNP | ((390, 'YRNQ'), '[CREATED]') |
| 2 | SIGLEC6 (CD327) | rs761002709 | < 0.01 | G/A | F4/80-hi CD11b-lo CD11c- B220- Macrophages and CD11b+ Gr1+ 7/4hi Neutrophils from BM | O43699 | 398 | H->Y | SNP | ((398, 'YQHQ'), '[CREATED]') |
| 3 | ABHD6 | rs771843813 | < 0.01 | G/A | CD11c-int CD8a+ CD4+ B220+ Gr+ Plasmacytoid DC | Q9BV23 | 65 | R->Q | SNP | ((62, 'YSFQ'), '[CREATED]') |
| 4 | SLAF7 (CD319) | rs765616054 | NA | A/G | CD11c+ CD8a+ CD4- CD11b- DC | Q9NQ25 | 261 | E->Q | SNP | ((258, 'YIEQ'), '[CREATED]') |
| 5 | PGFRB (CD140b) | rs140081345 | < 0.01 | C/T | CD117+ IL7R- CD150- CD48- AA4.1+ CD43+ HSC BM cells | P09619 | 565 | R->Q | SNP | ((562, 'YEIQ'), '[CREATED]') |
| 6 | VASN | rs766817153 | NA | G/A | CD117+ IL7R- CD150- CD48- AA4.1+ CD43+ HSC BM cells | Q6EMK4 | 600 | R->Q | SNP | ((597, 'YCVQ'), '[CREATED]') |
| 7 | ITB7 | rs149623424 | < 0.01 | C/T | CD4, CD8 and GFP+ (Foxp3 KI mice) CD4+ CD25+ Tregs | P26010 | 756 | R->Q | SNP | ((753, 'YDRQ'), '[CREATED]') |
| 8 | GYPC (CD236) | rs200062204 | < 0.01 | A/C | CD115+ MHC+ F4/80-lo, SiglecF-, CD11c+ Macrophages | P04921 | 88 | K->Q | SNP | ((85, 'YRHQ'), '[CREATED]') |
| 9 | C1QR1 (CD93) | rs752043162 | < 0.01 | C/T | CD115+ MHCII+ Ly6C+ CD11c+ Macrophages and AA4+ IgM- CD19+ CD43- HAS+ pre-B cells | Q9NPY3 | 609 | R->Q | SNP | ((606, 'YRKQ'), '[CREATED]') |
| 10 | SIT1 | rs761803789 | < 0.01 | A/T | CD3e+ CD4+ CD8- CD19- CD62L-hi naïve T cells and OT1tg Nave CD8 T cells | Q9Y3P8 | 93 | L->Q | SNP | ((90, 'YGNQ'), '[CREATED]') |
| 11 | TMIE | rs767118682 | < 0.01 | G/A | TCR-hi CD4- CD8+ CD24- mature T cells | Q8NEW7 | 96 | R->Q | SNP | ((93, 'YLQQ'), '[CREATED]') |
| 12 | TACT (CD96) | rs777279191 | < 0.01 | G/A | CD4, CD8, NK cells, gdT cells | P40200 | 544 | C->Y | SNP | ((544, 'YQYQ'), '[CREATED]') |

| | | | | | | | | | | |
|---|---|---|---|---|---|---|---|---|---|---|
| 13 | FGFR4 (CD334) | rs351855 | 0.3 | G/A | CD45+ MHCII+ CD11c+ CD11b+ DC cells, GFP+ (Foxp3 KI mice) CD4+ CD25+ Tregs | P22455 | 388 | G→R | SNP | ((388, 'YRGQ'), '[EXPOSED]') |
| 14 | TNFRSF4 (OX40) | rs776902723 | < 0.01 | C/T | CD19+ B220+ IgM++ AA4- CD23- CD43+ CD5+ B cells | P43489 | 241 | R->Q | SNP | ((238, 'YLLQ'), '[CREATED]') |
| 15 | SPIT2 | rs148652374 | < 0.01 | G/A | CD45+ MHCII+ CD11c+ CD11b+ DC cells, GFP+ (Foxp3 KI mice) CD4+ CD25+ Tregs | O43291 | 222 | R->Q | SNP | ((219, 'YLIQ'), '[CREATED]') |
| 16 | STIM1 | rs200849173 | NA | C/T | GFP+ (Foxp3 KI mice) CD4+ CD25+ Tregs | Q13586 | 259 | H->Y | SNP | ((259, 'YDLQ'), '[CREATED]') |
| 17 | CADM3 | rs771266619 | < 0.01 | G/A | CD11c+ CD8a- CD4+ CD11b+ | Q8N126 | 357 | R->Q | SNP | ((354, 'YLIQ'), '[CREATED]') |
| 18 | ERBB3 (HER3) | rs765179217 | < 0.01 | G/A | CD11c-int CD8a+ CD4+ B220+ Gr+ Plasmacytoid DC | P21860 | 683 | R->Q | SNP | ((680, 'YLEQ'), '[CREATED]') |
| 19 | ITA8 | rs561911227 | < 0.01 | C/A | CD11c+ CD4- CD11b- CD8+ DC | P53708 | 1051 | D->Y | SNP | ((1051, 'YREQ'), '[CREATED]') |
| 20 | ITB4 (CD104) | rs756905048 | < 0.01 | G/A | CD45+ MHCII+ CD11c+ CD11b+ DC cells | P16144 | 765 | R->Q | SNP | ((762, 'YMLQ'), '[CREATED]') |
| 21 | DCBD2 | rs115330244 | < 0.01 | C/T | CD115+ MHC+ F4/80-lo, SiglecF-, CD11c+ Macrophages | Q96PD2 | 572 | R->Q | SNP | ((569, 'YWDQ'), '[CREATED]') |
| 22 | EPHA4 | rs770032654 | < 0.01 | G/A | CD45+ MHCII+ CD11c+ CD11b+ DC cells | P54764 | 588 | H->Y | SNP | ((588, 'YLNQ'), '[CREATED]') |
| 23 | LRC25 | rs771704758 | < 0.01 | C/T | CD45+ MHCII+ CD11c+ CD11b+ DC cells, CD115+ B220- Ly6c+ MHCII+ Monocytes, CD115+ MHC+ F4/80-lo, SiglecF-, CD11c+ Macrophages | Q8N386 | 224 | R->Q | SNP | ((221, 'YGSQ'), '[CREATED]') |
| 24 | MPEG1 | rs780878835 | < 0.01 | C/T | CD45+ MHCII+ CD11c+ CD11b+ DC cells, CD115+ B220- Ly6c+ MHCII+ Monocytes, CD115+ MHC+ F4/80-lo, SiglecF-, CD11c+ Macrophages | Q2M385 | 680 | R->Q | SNP | ((677, 'YGTQ'), '[CREATED]'),((708, 'YQEQ'), '[PRESENT]') |

| | | | | | | | | | | |
|---|---|---|---|---|---|---|---|---|---|---|
| 25 | OSTM1 | rs780259047 | < 0.01 | G/A | CD45+ MHCII+ CD11c+ CD11b+ DC cells, CD115+ B220- Ly6c+ MHCII+ Monocytes, CD115+ MHC+ F4/80-lo, SiglecF-, CD11c+ Macrophages | Q86WC4 | 306 | H->Y | SNP | ((306, 'YSEQ'), '[CREATED]') |
| 26 | SDC3 | rs775969974 | < 0.01 | C/A | CD45+ MHCII+ CD11c+ CD11b+ DC cells, CD115+ B220- Ly6c+ MHCII+ Monocytes, CD115+ MHC+ F4/80-lo, SiglecF-, CD11c+ Macrophages | O75056 | 422 | E->Q | SNP | ((419, 'YTLQ'), '[CREATED]') |
| 27 | CD68 | rs370867284 | < 0.01 | C/T | CD45+ MHCII+ CD11c+ CD11b+ DC cells, CD115+ B220- Ly6c+ MHCII+ Monocytes, CD115+ MHC+ F4/80-lo, SiglecF-, CD11c+ Macrophages | P34810 | 349 | S->Y | SNP | ((349, 'YAYQ'), '[CREATED]') |
| 28 | IL6RB (CD130) | rs200816863 | < 0.01 | G/A | TCR+ CD4- TCRa/b CD122-hi CD44-hi CD25- CD8+ T cells | P40189 | 662 | H->Y | SNP | ((662, 'YIAQ'), '[CREATED]') |
| 29 | LAMP5 | rs781664839 | < 0.01 | G/T | CD45+ MHCII+ CD11c+ CD11b+ DC cells | Q9UJQ1 | 272 | D->Y | SNP | ((272, 'YRSQ'), '[CREATED]') |
| 30 | RON (CD136) | rs375697146 | < 0.01 | C/T | CD115+ MHCII+ F4/80-lo, SiglecF-, CD11c+ Macrophages | Q04912 | 983 | R->Q | SNP | ((980, 'YWWQ'), '[CREATED]') |
| 31 | SEM6D | rs370361613 | < 0.01 | G/A | F4/80-hi CD11b-lo CD11c- B220- Macrophages | Q8NFY4 | 687 | R->Q | SNP | ((684, 'YCYQ'), '[CREATED]') |
| 32 | AXL | rs775803336 | < 0.01 | G/A | CD45+ MHCII+ CD11c+ CD11b+ DC and F4/80-hi CD11b-lo CD11c- B220- Macrophages | P30530 | 507 | R->Q | SNP | ((504, 'YSRQ'), '[CREATED]') |
| 33 | FCGR1B (CD64) | rs587642032 | < 0.01 | C/T | CD115+ B220- Ly6c+ MHCII+ Monocytes | Q92637 | 245 | S->Y | SNP | ((245, 'YSLQ'), '[CREATED]') |
| 34 | CD302 | rs769756355 | < 0.01 | - / T | F4/80-hi CD11b-lo CD11c- B220- Macrophages | Q8IX05 | 196 | H->Q | frame shift | ((193, 'YKKQ'), '[CREATED]') |

| | | | | | | | | | | |
|---|---|---|---|---|---|---|---|---|---|---|
| 35 | MEGF9 | rs185776336 | < 0.01 | C/T | Bone Marrow CD11b+ Ly6-G+ Granulocytes | Q9H1U4 | 544 | R->Q | SNP | ((541, 'YQNQ'), '[CREATED]') |
| 36 | VOPP1 | rs760304705 | < 0.01 | C/A | CD3- NK1.1+ Ly49C/I+ NK cells | Q96AW1 | 89 | P->Q | SNP | ((86, 'YPPQ'), '[CREATED]'),( (100, 'YTRQ'), '[PRESENT]') |
| 37 | TMIGD2 (CD28H) | rs763256697 | < 0.01 | G/A | CD4, CD8 T cells | Q96BF3 | 200 | R->Q | SNP | ((197, 'YRPQ'), '[CREATED]') |
| 38 | X3CL1 | rs199662906 | < 0.01 | G/A | CD45+ MHCII+ CD11c+ CD11b+ DC cells | P78423 | 385 | R->Q | SNP | ((382, 'YIPQ'), '[CREATED]') |
| 39 | SYT15 | rs201199533 | < 0.01 | A/G | | Q9BQS2 | 53 | S->Y | SNP | ((53, 'YSGQ'), '[CREATED]') |
| 40 | ACE (CD143) | rs765069550 | < 0.01 | C/T | | P12821 | 1293 | H->Y | SNP | ((1293, 'YGPQ'), '[CREATED]') |
| 41 | AMHR2 | rs150262652 | < 0.01 | G/A | CD4+CD25+Tregs | Q16671 | 178 | R->Q | SNP | ((175, 'YRVQ'), '[CREATED]') |
| 42 | CDHR5 | rs538921373 | < 0.01 | C/T | | Q9HBB8 | 697 | R->Q | SNP | ((694, 'YGPQ'), '[CREATED]') |
| 43 | CN037 | rs759882651 | < 0.01 | T/A | | Q86TY3 | 757 | N->Y | SNP | ((757, 'YSMQ'), '[CREATED]') |
| 44 | CSTN2 | rs140778211 | < 0.01 | G/A | | Q9H4D0 | 856 | R->Q | SNP | ((853, 'YRVQ'), '[CREATED]') |
| 45 | DCC | rs765644105 | < 0.01 | C/A | | P43146 | 1125 | S->Y | SNP | ((1125, 'YSAQ'), '[CREATED]') |
| 46 | EREG | rs35275884 | < 0.01 | G/A | CD+CD25+ Tregs | O14944 | 147 | R->Q | SNP | ((144, 'YRNQ'), '[CREATED]') |
| 47 | ERN2 | rs775764629 | < 0.01 | G/A | | Q76MJ5 | 474 | H->Y | SNP | ((474, 'YISQ'), '[CREATED]') |
| 48 | GLPE | rs17018900 | < 0.01 | C/T | | P15421 | 78 | R->Q | SNP | ((75, 'YCIQ'), '[CREATED]') |
| 49 | IZUM1 | rs778368561 | < 0.01 | C/A | | Q8IYV9 | 346 | D->Y | SNP | ((346, 'YSRQ'), '[CREATED]') |

| | | | | | | | | | | |
|---|---|---|---|---|---|---|---|---|---|---|
| 50 | K1644 | rs146886645 | < 0.01 | C/T | | Q3SXP7 | 134 | R->Q | SNP | ((131, 'YLAQ'), '[CREATED]') |
| 51 | LRFN3 | rs529471562 | < 0.01 | C/G | | Q9BTN0 | 565 | H->Q | SNP | ((562, 'YKVQ'), '[CREATED]') |
| 52 | LRRT4 | rs775079691 | NA | G/T | | Q86VH4 | 473 | S->Y | SNP | ((473, 'YERQ'), '[CREATED]') |
| 53 | MMP24 | rs149443021 | < 0.01 | G/A | | Q9Y5R2 | 639 | R->Q | SNP | ((636, 'YYKQ'), '[CREATED]') |
| 54 | NTRK3 | rs568926009 | NA | C/T | | Q16288 | 459 | R->Q | SNP | ((456, 'YGRQ'), '[CREATED]') |
| 55 | SEM5A | rs138316526 | < 0.01 | G/A | | Q13591 | 995 | R->Q | SNP | ((992, 'YCQQ'), '[CREATED]'),( (996, 'YQQQ'), '[PRESENT]') |
| 56 | SIM14 | rs138349269 | < 0.01 | G/A | | Q96QK8 | 88 | H->Y | SNP | ((88, 'YNGQ'), '[CREATED]') |
| 57 | ZP4 | rs768615983 | < 0.01 | C/T | | Q12836 | 534 | C->Y | SNP | ((534, 'YPDQ'), '[CREATED]') |
| 58 | CADH1 (CD324) | Rs587783048 / rs587782162 | NA / < 0.01 | C/- and C/T | | P12830 | 731 | L->* | frame shift | ((741, 'YCPQ'), '[CREATED]') |

# Methods

**Study approval.** All of the experimental protocols were performed under protocols approved and reviewed by the Institutional Animal Care and Use Committee at the Max Planck Institute of Biochemistry, Am Klopfersptiz 18, Martinsried 82152 and the Institutional Animal Care and Use Committees at the University of Miami Miller School of Medicine, Miami, FL 33101.

**Statistical analysis.** The differences between the means of the wild-type and mutant groups were determined using 2-tailed unpaired t-test. For two-group comparisons, the Mann-Whitney rank-sum test or unpaired t-test with welch correction were used. For multiple group comparisons, two-way ANOVA with sidak's or tukey's comparison test was used. The criterion for statistical significance namely $p < 0.05$. A value of $p < 0.05$, $p < 0.001$ and $p < 0.0001$ were denoted by *, ** and *** respectively. All data were represented as means ±SD or ±SEM. Statistical analysis was performed using Graphpad Prism, version 7.01 (GraphPad Software).

**Animal models.** All mice used for this study were raised in C57BL/6 background. *Fgfr4* knock-in mice previously described (Cancer Res; 70(2); 802–12) used at 8-10 weeks of age. Foxp3-GFP knock in reporter mice was kindly provided by Dr. Kerstin Berer & Dr. Gurumoorthy Krishnamoorthy, Max Planck Institute of Neurobiology, Martinsried, Germany.

A knock-in mouse model for non-small cell lung cancer was generated by breeding $Fgfr4^{rs351855\text{-}A/A}$ and $Fgfr4^{rs351855\text{-}G/G}$ mice with *SPC-CRAF-BxB* mice as described previously (Nature **528**, 570-574). The breeder pairs were kindly provided by Prof. Ulf R. Rapp, Max Planck Institute of Heart and Lung Research, Bad-Nauheim, Germany. *SPC-Craf BxB* induce lung tumors in alveolar type II cells of the lung that can be analyzed from 4 months of age. Five to six months old mice were genotyped and sacrificed for analyses.

A knock-in mouse model for breast cancer was generated by breeding $Fgfr4^{rs351855\text{-}A/A}$ and $Fgfr4^{rs351855\text{-}G/G}$ mice with *WAP-Tgfα* mice as previously described (Nature **528**, 570-574). Only female mice post pregnancy were analyzed. Flow cytometry analyses involving cohorts of wild-type and risk-variant groups of mice were done by sacrificing all the mice on the same day.

All lung cancer and breast cancer mouse models used for tumor analyses were male and females respectively. Tumor-bearing mice were regularly monitored and killed before tumor burden affected their well-being. In the *WAP-Tgfα* transgenic mouse models for breast cancer, spontaneous tumors that arise in mammary pads are visible and measurable. As per our legal institute permit, the maximum tumor volume permitted in *WAP-Tgfα* mouse models of breast cancers was 1.500 $mm^3$ (single tumors); in none of our experiments were these limits exceeded. In the *SPC-Craf-BxB* transgenic mouse models for non-small-cell lung cancer, the spontaneous tumor in vivo does not permit measurement in live animals. However, loss of body weight is proportional to tumor burden. The maximum weight loss permitted as per our animal permit was 10% of initial body weight. In none of our experiments with mouse models for lung cancer were these limits exceeded.

Immunophenotyping of *Fgfr4* knock-out mice. Male *Fgfr4* deficient mice and wild type littermates previously described (Cell Metabol; 22(6):1020-32) were sacrificed at 8 weeks of age and immune cells were prepared from thymus and spleen.

**Human population genotype data.** Human genotype data (germline and somatic) in the variable call formats were gathered and aggregated from publicly available datasets, namely HapMap release 28, Wellderly, dbSNP build 149, 1000 genomes ph3, ExAC.r0.3, NCI-60, TCGA, COSMIC and CCLE. Allele frequencies for germline data were obtained from 1000 genome phase 3 build.

**Computational Analyses.** Aggregated germline variant datasets and somatic variant datasets (mixing of germline genomic DNA from infiltrated immune cells is always a possibility) were analyzed using Transmembrane Protein Variant Identifier algorithm (TraPS-VarI). Results are available at https://vj-ulaganathan.github.io/TraPS_VarI_SourceData.html. TraPS VarI is a tool to identify membrane-proximal tyrosine-based sequence motifs YxxQ, where Y is tyrosine, Q is glutamine and x any amino acid. The python based module for identifying germline receptor variants of single-pass transmembrane proteins that are capable of modulating in a genotype-dependent manner the STAT3 signaling and drug sensitivity to growth inhibition (https://gitlab.com/VJ-Ulaganathan/TraPS-VarI). The algorithm requires single nucleotide polymorphism genotyping datasets in Variable Call Format 4.0 as input.

**Western blot analyses.** Whole cell lysates were prepared using 1X Cell Lysis Buffer (Cell Signaling #9803) containing cOmplete, mini, EDTA-free tablets (Roche # 11836170001) and PhosSTOP tablets (Roche #04906837001). Equal protein amounts (20-30 μg) were loaded after a (BCA) assay, were seperated on 4-15% Mini-PROTEAN TGX Gels (Bio-Rad # 456-1083) and subsequently transferred onto nitrocellulose membranes. Blots were blocked in 1X NET-Gelatin buffer (1.5 M NaCl, 0.05 M EDTA, 0.5 M Tris pH 7.5, 0.5 % Triton X-100 and 0.25 g/ml Gelatin) and incubated with primary antibodies overnight at 4º C.

The following antibodies were used for western blotting:

Rabbit anti-FGFR4 (Cell Signaling, #8562; clone-D3B12), rabbit anti-FGFR4 (C-16) (Santa Cruz, #sc-124), mouse anti-FGFR4 (A-10) (Santa Cruz, #sc-136988), rabbit anti-FGFR4 (H-121) (Santa Cruz, #sc9006), rabbit anti-ERK1/2 (Cell Signaling, #4695S; clone-137F5), rabbit anti-pERK1/2 (Cell Signaling, #4376S; clone-20G11), mouse anti-BrdU (Cell Signaling, #5292; clone-Bu20a), rabbit anti-pSTAT3 (Y705) (Cell Signaling, #9145; clone-D3A7), rabbit anti-pSTAT3 (S727) (Cell Signaling, #9134), rabbit anti-STAT3 (Cell Signaling, #4904; clone-79D7), mouse anti-STAT3 (Cell Signaling, #9139; clone-124H6), mouse anti-TUBULIN (Sigma, #9026; clone-DM1A), mouse anti-ADAM22 (BioLegend, #831001; clone-N57/2), rabbit anti-AMHR2 (Life Technologies, #PA5-13900), rabbit anti BMPR1b antibody (Merck-Millipore, #ABD50), rabbit anti-CSTN2 (USB life sciences, #034017), rabbit anti-EPIREGULIN (FL-162) (Santa Cruz, #sc-30215), rabbit anti-NTRK3 (Cell Signaling, #3376; clone-C44H5), rabbit anti-SEM5A (Life Technologies, #PA5-26066), rabbit anti-SPINT2 (Abcam, #ab128926; clone-EPR6283(2)) and FOXP3-HRP antibody (Biorbyt, #orb110190).

Horseradish peroxidase (HRP)-conjugated secondary antibodies, anti-rabbit conformation-specific HRP conjugated (Cell Signaling, #5127) and anti-mouse light chain-specific HRP conjugated (Dianova, # 115-035-003) antibodies along with an ECL kit (GE Healthcare/ Amersham Pharmacia Biotech, #32106) were used to detect protein signals. Multiple exposures were taken to select images within the dynamic range of the film (GE Healthcare Amersham Hyperfilm ECL, #28906838). Normalization was done using tubulin bands.

**Immunoprecipitation.** Transfectants were lysed in 1X Cell lysis buffer (Cell Signaling, #9803) containing containing cOmplete, mini, EDTA-free tablets (Roche # 11836170001) and PhosSTOP tablets (Roche #04906837001). Lysates were cleared and incubated with primary antibody overnight at 4º C. 50 µl of Dynabeads Protein A (#10006d, Life Technologies) was added per sample and incubated at rocking for additional 4 hours. Magnetic bead-bound proteins were separated using a DynaMag-2 magnet (#12321, Life Technologies). After 5 washes, co-immunoprecipitated proteins were extracted in 3X Laemmli Buffer.

**Flow cytometry.** Single cell suspensions from bone marrow, thymus, lymph nodes, spleen, lungs, blood and tumors were prepared for staining. Erythrolysis by ACK lysis buffer (1.5 M $NH_4Cl$, 100 mM $KHCO_3$, 10 mM EDTA-$Na_2$, pH 7.4) was performed for suspensions from blood, spleen and bone marrow. Single cell suspensions of whole lung and breast tissues as well as organ bearing tumors were performed by first slicing the tissue in small pieces and resuspending it in 10 mL of digestion cocktail [0.03 gms of Liberase TM (Roche, #05401119001) and 1.3 mg of DNAse I (Thermo Scientific, #EN0521)] reconstituted in RPMI complete medium. Digestion was performed by gentle agitation at 37º C for 30 minutes.

Single cell suspensions were stained with the following antibodies: Rat IgG2b-FITC/Rat IgG2a-RPE negative control (AbD Serotec, #DC037), rat anti-Mouse CD4-FITC/CD8-RPE (AbD Serotec, #DC034; clone-YTS191.1/KT15), rat anti-CD19-RPE (AbD Serotec, #MCA1439PET; clone- 6D5), rat anti-Mouse F4/80-FITC (BioRad, #MCA497FT; clone-Cl:A3-1), rat anti-mouse CD4-PE (eBioscience, #12-0042-81; clone-RM4-5), rat anti-mouse CD8a-PE (eBioscience, #12-0081-81; clone-53-6.7), rat anti-mouse CD25-PerCP-Cy5.5 (eBioscience, #45-0251-82; clone-PC61.5), rat anti-mouse NKp46-PE (eBioscience, #12-3351; clone-29A1.4), rat IgG2a Isotype Control PE (eBioscience, #12-4321; clone-eBR2a), rat anti-mouse CD49b-APC (eBioscience, #17-5971; clone-DX5), armenian hamster anti-mouse CD3e-FITC (eBioscience, #11-0031; clone-145-2C11), armenian Hamster IgG Isotype Control APC (eBioscience, #17-4888; clone-eBio299Arm), armenian hamster anti-mouse gamma delta TCR-APC (eBioscience, #17-5711-81; clone-eBioGL3 (GL-3, GL3)), rat anti-mouse CD117-APC (eBioscience, #17-1171-82; clone-2B8), rat anti-mouse IL7R-FITC (eBioscience, #11-1271-81; clone-A7R34), rat anti-mouse CD150-PE (eBioscience, #12-1502-82; clone-mShad150), armenian hamster anti-mouse CD48-biotin (eBioscience, #13-0481-81; clone-HM48-1), armenian Hamster IgG Isotype Control, Biotin (eBioscience, #13-4888-81; eBio299Arm), rat anti-mouse CD93 (AA4.1)-biotin (eBioscience, #13-5892-81; clone-AA4.1), rat IgG2b kappa Isotype Control, Biotin (eBioscience, # 13-4031-82; clone-eB149/10H5), rat anti-mouse CD43-biotin (eBioscience, #13-0431-82; clone-eBioR2/60), rat IgM Isotype Control, Biotin (eBioscience, #13-4341-81; clone-eBRM), rat anti-mouse CD11b-APC (eBioscience, #17-0112-81; clone-M1/70), armenian hamster anti-mouse CD11c-PE (eBioscience, #12-0114-81; clone-N418), armenian Hamster IgG Isotype Control, PE (eBioscience, #12-4888-81; clone-eBio299Arm), rat anti-mouse B220-FITC (eBioscience, #11-0452-63; clone-RA3-6B2), rat anti-mouse Gr1-PerCP (Novus Biologicals, #FAB1037C-100; clone-RB6-8C5), rat anti-mouse CD115-FITC (eBioscience , #14-0112-82; clone-M1/70), rat anti-mouse MHCII-APC (eBioscience , #17-5321-82; clone-M5/114.15.2), rat anti-mouse Ly6C-PE (eBioscience, #12-5932-80; clone-HK1.4), rat anti-mouse IgM-biotin (eBioscience, #13-5790-82; clone-II/41), rat IgG2a kappa Isotype Control,

Biotin (eBioscience, #13-4321-82; clone-eBR2a) rat anti-mouse CD24 (HAS)-PerCP-Cy5.5; , #45-0242-82; clone-M1/69), rat anti-mouse CD62L-APC (eBioscience , #17-0621-81; clone-MEL-14), rat anti-mouse CD5-PE (eBioscience , #12-0051-82; clone-53-7.3), rat anti-mouse CD45-PerCP (eBioscience, #MA1-10234; clone-EM-05), rat anti-mouse CD170 (SiglecF) (eBioscience , #14-1702-82; clone-1RNM44N), rat anti-mouse Ly6-G;-biotin (eBioscience , #13-5931-82; clone-RB6-8C5), mouse anti-mouse NK1.1-FITC (eBioscience , #11-5941-81; clone- PK136), mouse IgG2a kappa Isotype Control, FITC (eBioscience, #11-4724-81; clone-eBM2a), syrian hamster anti-mouse Ly49C/1-biotin (eBioscience , #13-5991-81; clone- 14B11), syrian Hamster IgG Isotype Control, Biotin (eBioscience, #13-4914-81), rat anti-mouse CD14-PerCP (eBioscience , #11-0141-81; clone-Sa2-8), armenian hamster anti-mouse CD80-biotin (eBioscience , #13-0801-81; clone-16-10A1) and rat anti-mouse CD86-biotin (eBioscience , #13-0862-81; clone-GL1).

Secondary detection reagents were as follows; Goat anti-Human-APC (Dianova, #109-136-088), donkey anti-Mouse-DyLight488 (Dianova, #715-485-150), goat anti-Rabbit-APC (Dianova, #111-136-144), goat anti-Mouse-APC (Dianova, #115-136-146) and fluorochrome conjugated streptavidin namely PE/Cy7 Streptavidin (BioLegend, #405206), Brilliant Violet 421 Streptavdin (BioLegend, #405226), Brilliant Violet 510 (BioLegend, #504233 and Brilliant Violet 605 (BioLegend, #405229. Rabbit anti-FGFR4 antibody (#136988, Santa Cruz) was directly conjugated with PerCP Cy5.5 using PerCP Cy5.5 conjugation kit (#LNK142PERCPCY5.5 CJ, AbD Serotec).

Data was analyzed using Flojo Software vX.0.7.

**ELISA.** IL10 levels in equal volumes of mouse serum samples were quantified using mouse IL10 ELISA ready-set-go kits (eBioscience, #887104-22) by following instructions of the manufacturer.

**Immunohistochemistry and immunofluorescence.** Tissues were fixed overnight in 4% paraformaldehyde in PBS (pH 7.4) at 4º C. Fixed tissues were embedded in paraffin and sliced. Sections were prepared for staining first by deparaffinization followed by hydration in the following solutions: 3 washes of xylene 5 minutes each, two washes of 100% ethanol 10 minutes each, two washes of 95% ethanol 10 minutes each and two washes in distilled water 5 minutes each. Antigen retrieval was obtained by incubation with heated citrate buffer (sodium citrate 10mM, pH 6) for 15 minutes. Immunohistochemistry was performed as per our standard procedures. Briefly, after antigen retrieval sections were incubated 3% hydrogen peroxide for 10 minutes to quench endogenous peroxidase activity. Non-specific background staining was blocked by incubating in UltraVision Block (Thermo Scientific, # TA-060-PBQ) for 5 minutes at room temperature. Ki67 staining was done by incubating in rabbit anti-Ki67 mAb (Cell Signaling, #9027) at a dilution of 1: 400 overnight at 4º C and CD8 TIL staining was achieved using biotin rat anti-mouse CD88a (BD Pharmingen, #553029, clone-53-6.7 after Fc receptor blocking by mouse 8D Fc block (BD Pharmingen, #553141, clone-2.4G2). For isotype control staining biotin rat IgG2a, κ isotype (BD Pharmingen, #553928) was used. Detection was achieved using HRP Polymer (Thermo Scientific, # TL-060-PH) followed by incubation with peroxidase compatible DAB chromogen.

For immunofluorescence, anti-mouse CD8a-FITC, clone 53-6.7 (eBioscience, # 11-0081-82) was used.

**Real Time RT-PCR.** Total RNA was isolated using RNeasy Kit (Qiagen, #74104). RNA was reverse transcribed into cDNA by random hexamer with First Strand cDNA Synthesis Kit (Thermo Scientific,

#K1622). A StepOne Plus Real Time PCR System (Applied Biosystem) and Fast SYBR Green Master Mix (Life Science Technologies, #4385612) were used for quantitative RT-PCR. Primers used were as follows: mouse *Fgfr4* (forward: 5'-CAAGTGGTTCGTGCAGAGG-3' and
Reverse: 5'-CTTCATCACCTCCATCTCGG-3'),
*Cd4* (forward: 5'-CGAACATCTGTGAAGGCAAA-3' and
reverse: 5'- GAGCTCTTGTTGGTTGGGAA-3'),
*Cd8* (forward: 5'- GATTGGACTTCGCCTGTGAT-3' and
reverse: 5'- CTTGCCTTCCTGTCTGACTA-3'),
*Foxp3* (forward: 5'- GCGAAAGTGGCAGAGAGGTA-3' and
reverse: 5'- GAGGAGCTGCTGAGATGTGA-3'),
*Il10* (forward: 5'-TTTGAATTCCCTGGGTGAGA-3' and
reverse: 5'-AGACACCTTGGTCTTGGAGC-3') and
*Hprt* (forward: 5'- CTTCCTCCTCAGACCGCTTT-3' and
reverse, 5'- TTTTCCAAATCCTCGGCATA-3')

**Purification of CD8 and Tregs.** CD8+ve T cells, CD4+CD25-Teffector cells and CD4+CD25+ Treg cells were isolated from spleens of mice groups of *Fgfr4*$^{rs351855\text{-}G/G}$ and *Fgfr4*$^{rs351855\text{-}A/A}$ genotypes. For each isolation procedures a group consisted of 7 mice. Mice were age and gender matched. For immunoblot analysis of purified CD8+ve T cells, CD4+CD25- Teffector cells and CD4+CD25+ Treg cells, 8-week old wild type C57Bl/6 mice were used for isolation (n = 15 mice). Purified cells were lysed immediately in 1X Cell Lysis Buffer (#9803, Cell Signaling). All steps taken during isolation procedures were followed as per the manufacturer's guidelines described in Dynabeads® FlowComp™ Mouse CD8 Kit (#11462D, Life Technologies) and Dynabeads® FlowComp™ Mouse CD4+CD25+ Treg Cells Kit (#11463D, Life Technologies).

**Generation of bone marrow derived macrophages (BMDM) and dendritic cells (BMDC).** The femur bones from both legs of adult mice were carefully rinsed in 70% ethanol before flushing them with cold incomplete medium. The flushes were collected in a centrifugation tube and washed with 50 mL incomplete medium. After ACK erythrolysis cells were washed once in complete RPMI with 10% FCS and 2.5 x $10^6$ cells were cultivated in a bacteriological Petri dishes (for non-adhesive surface) in 10 mL complete medium. For BMDM, 1 mL of L929 conditioned medium was added per 10 mL dish on day 0. On day 3, 8 mL of culture medium was replaced with 10 mL fresh conditioned medium (8 mL RPMI with10% FCS and 2 mL L929 medium). On day 6, non-adherent cells were removed and medium was replaced with fresh complete medium. BMDM were harvested on day 8 and lysed for immunoblot analyses. An aliquot was taken for FACS staining using antibodies against CD14, CD11b, CD11c, CD3, CD19, MHCII, CD80 and CD86.

For BMDC, 1 mL of GM-CSF producing hybridoma conditioned medium was added to 10 mL bone marrow culture on day 0. On day 3, medium was replaced with 8 mL RPMI with 10% FCS and 2 mL GM-CSF producing hybridoma conditioned medium. On day 6, old culture medium was once again exchanged with 8 mL RPMI with 10% FCS and 2 mL GM-CSF producing hybridoma conditioned medium. On day 8, BMDC were harvested for immunoblot analyses. An aliquot was taken for FACS staining using antibodies against CD14, CD11b, CD11c, CD3, CD19, MHCII, CD80 and CD86.

**In vitro TREG suppression assay.** Treg suppression capacity was evaluated by according to a protocol by Vignali and Colleagues (Methods Mol Biol. (2011; 707: 21–37) with slight modifications. Purified CD8, CD4+CD25+Teff and CD4+CD25+Tregs were assessed for purity followed by staining with proliferation markers, CFSE (#C34554, Life Technologies) for CD8 & Teffs and eFluor670 (#65-0840-85, eBisocience) for Tregs. Counted cells were plated in U-bottomed 96-well plates in desired ratios with same volume of Dynabeads® Mouse T-Activator CD3/CD28 for T-Cell Expansion and Activation (#11456D, Life Technologies) either in presence or absence of mouse IL10 neutralizing antibody, clone JES5-2A5 (#16-7102-81, eBioscience). Relative numbers of CFSE labeled and eFluor670 labeled cells were counted at start and end of experiment viz, day 0 and day 3 respectively using calibrate beads. Percent suppression was calculated using the following formula: ((Numbers of CD8 T cells alone – Numbers of CD8 T cells co-cultivated with $T_{REGs}$)/Numbers of CD8 T cells alone) X 100. To determine statistical significance between groups, two-way ANOVA with a confidence interval of 95% was used.

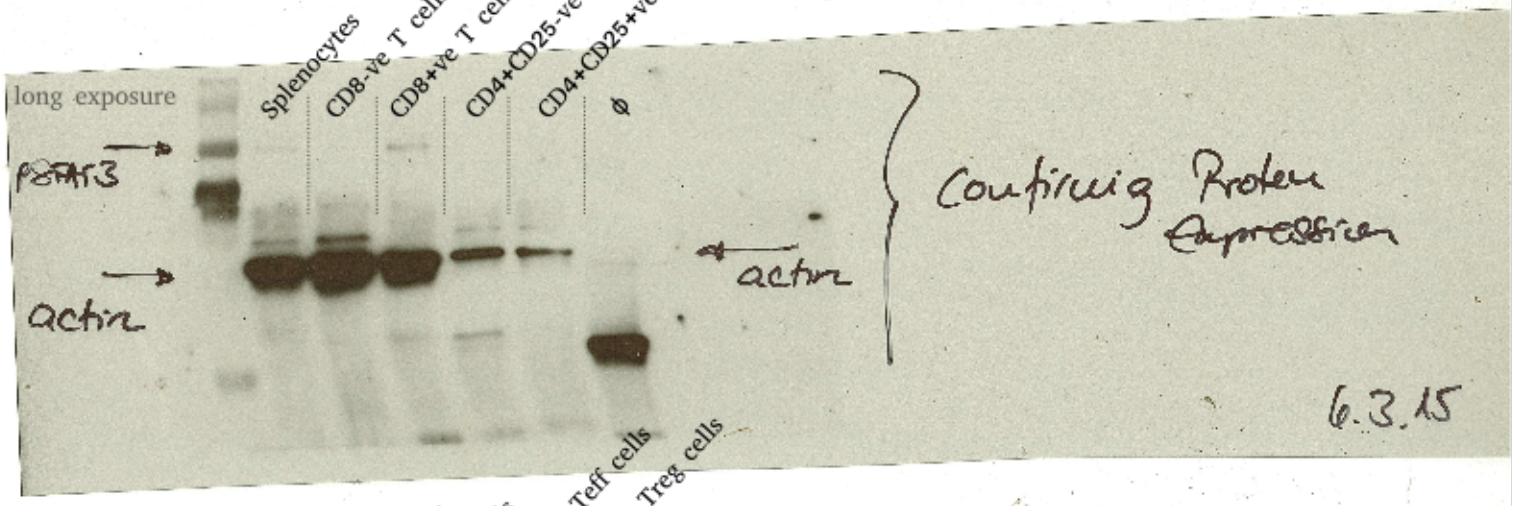


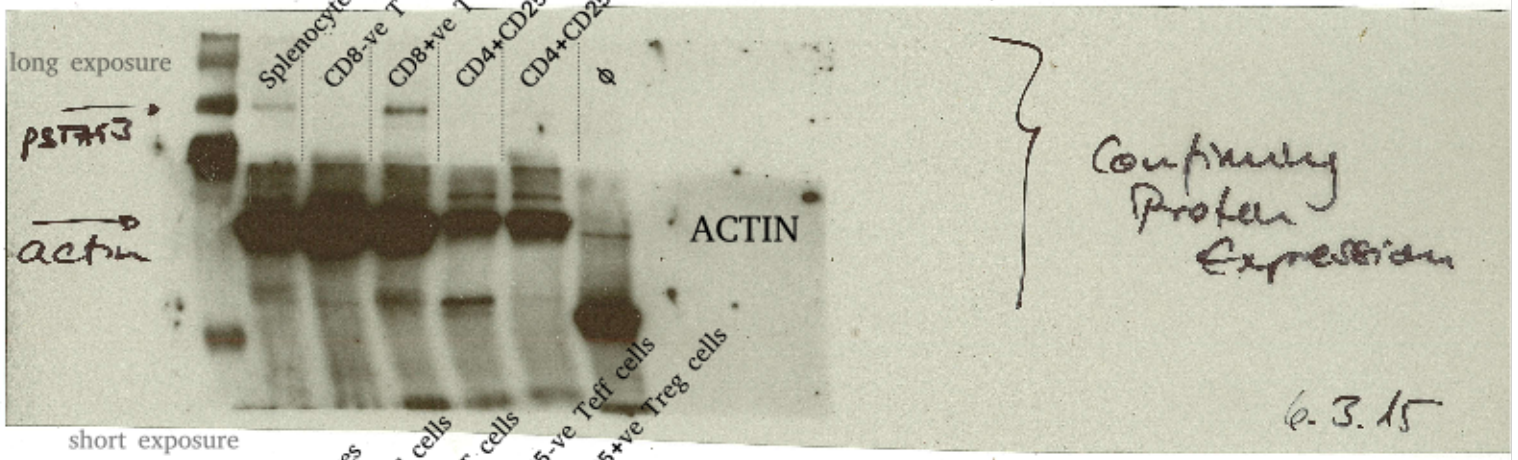


short exposure

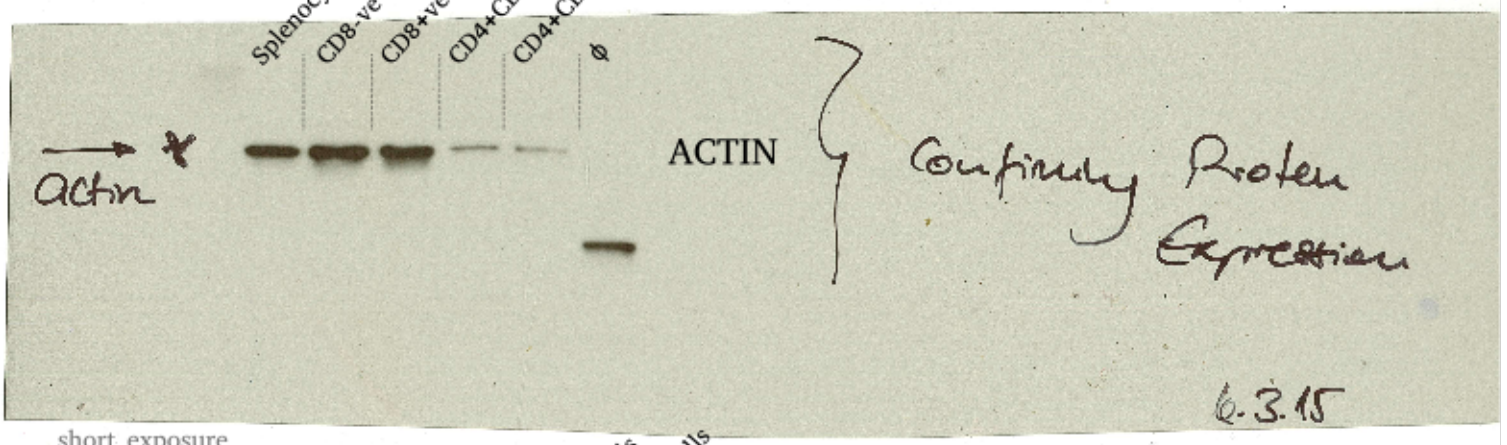


short exposure

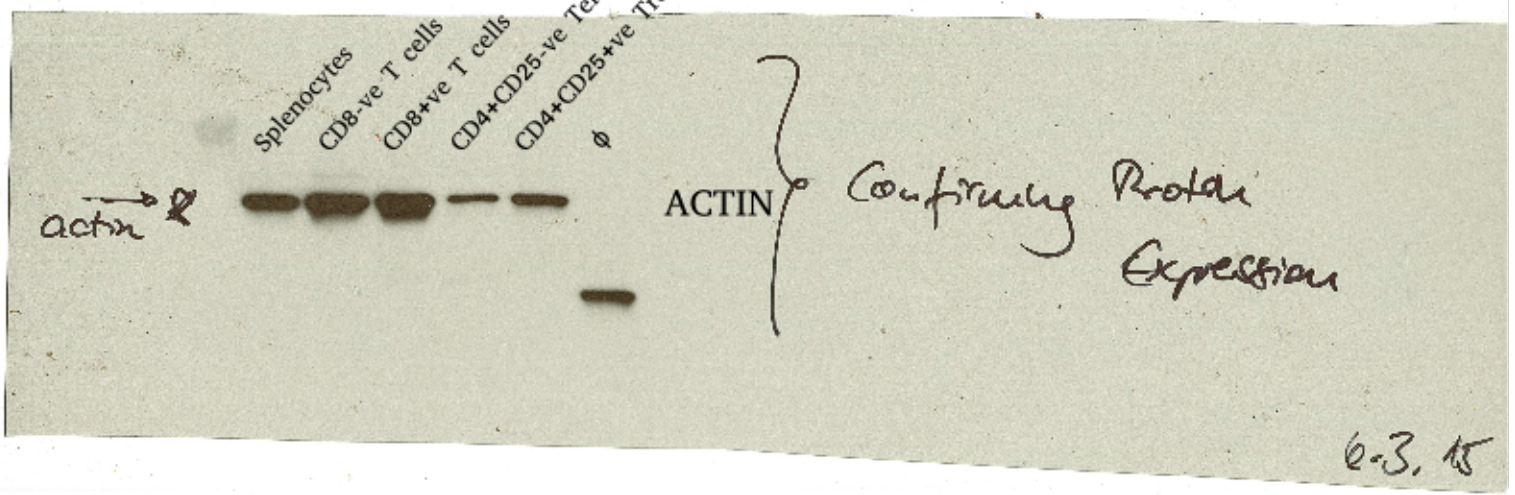

# UNCUT GELS PERTAINING TO FIGURE 1A

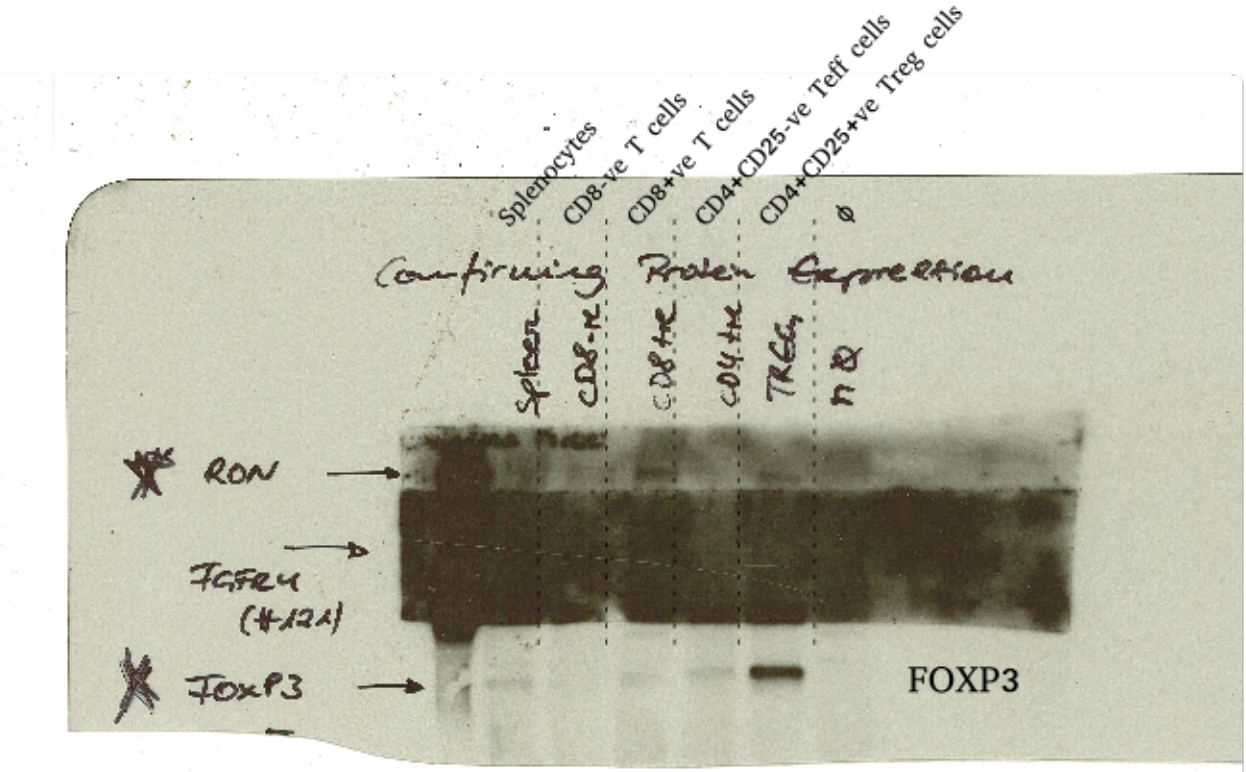


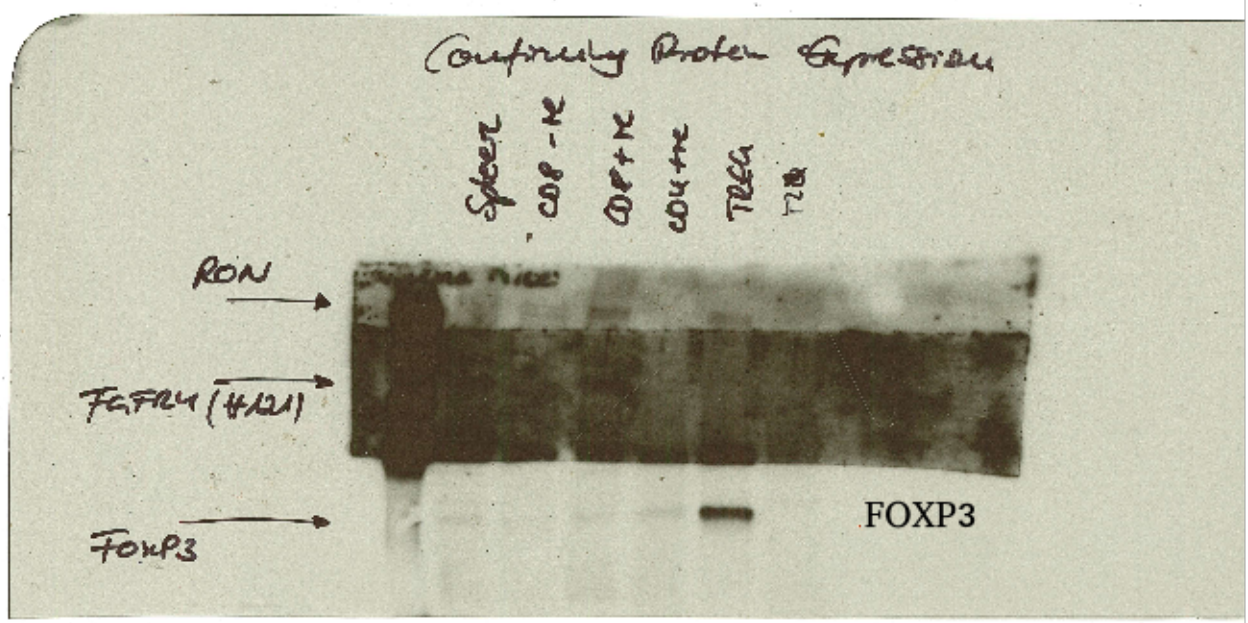

# UNCUT GELS PERTAINING TO FIGURE 1A

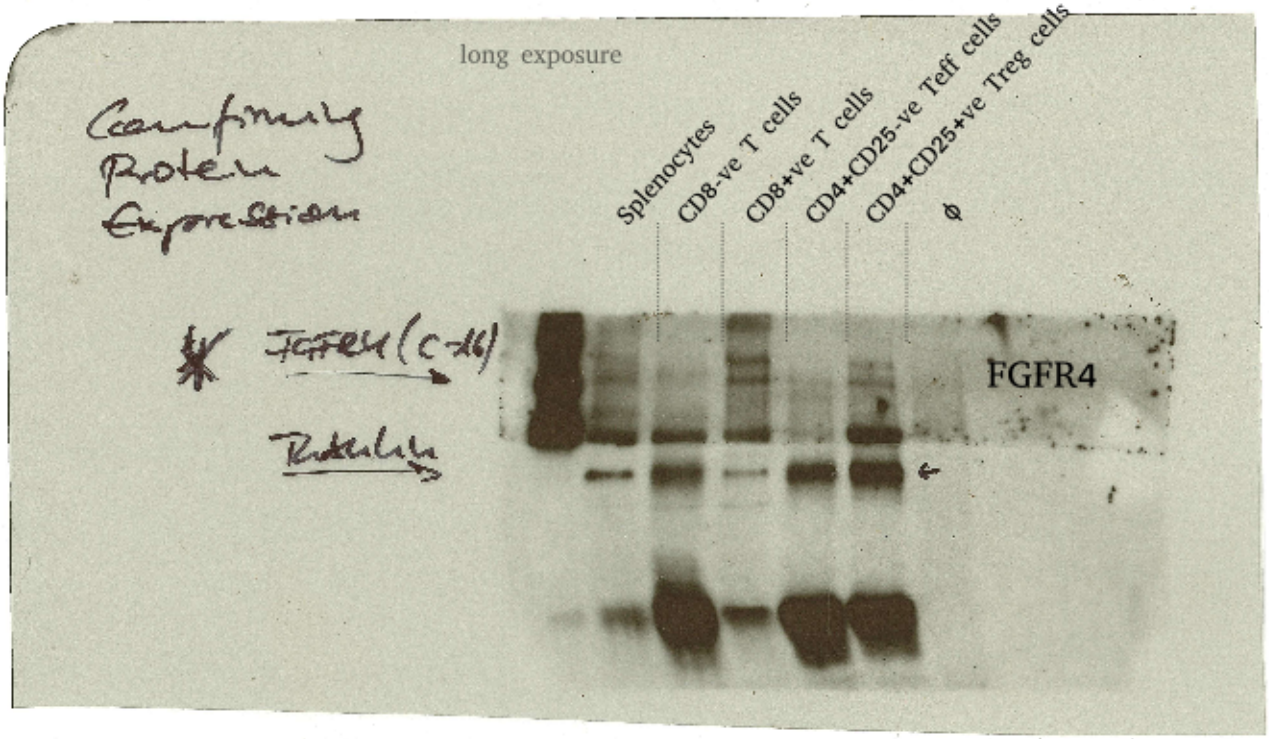


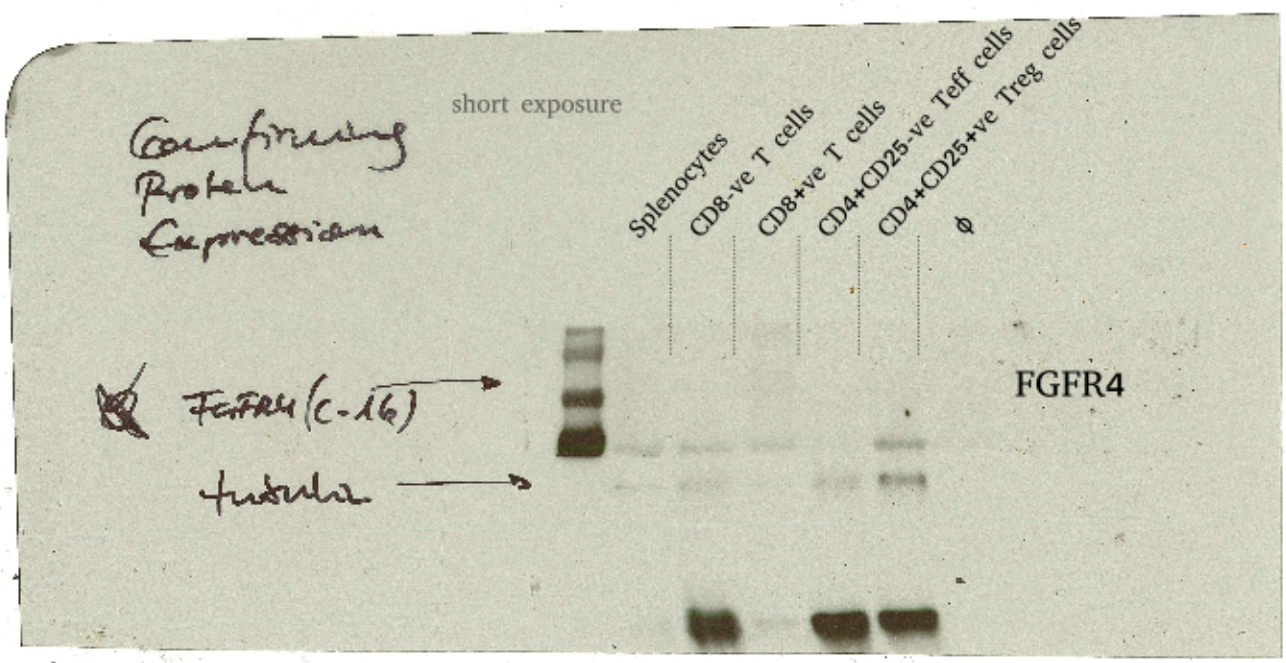

# UNCUT GELS PERTAINING TO SUPPLEMENTAL FIGURE 1C


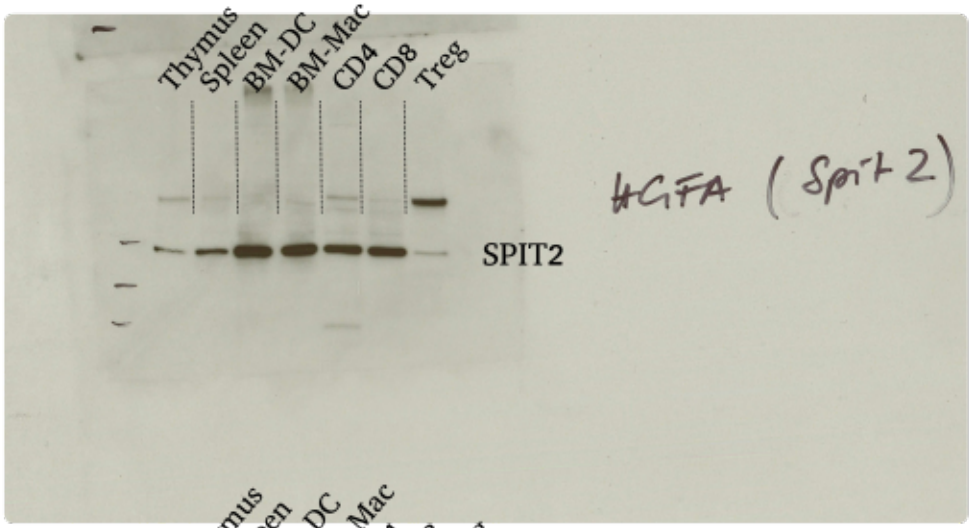


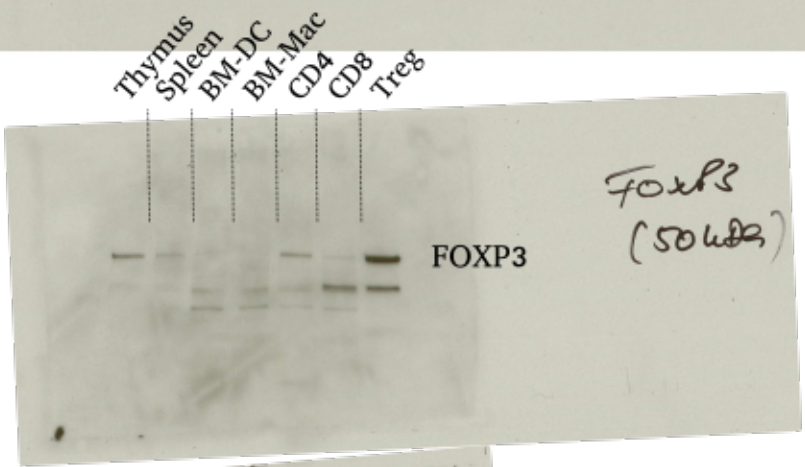


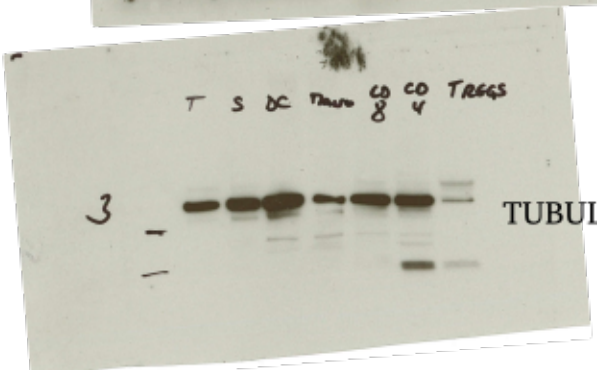

# UNCUT GELS PERTAINING TO SUPPLEMENTAL FIGURE 1C

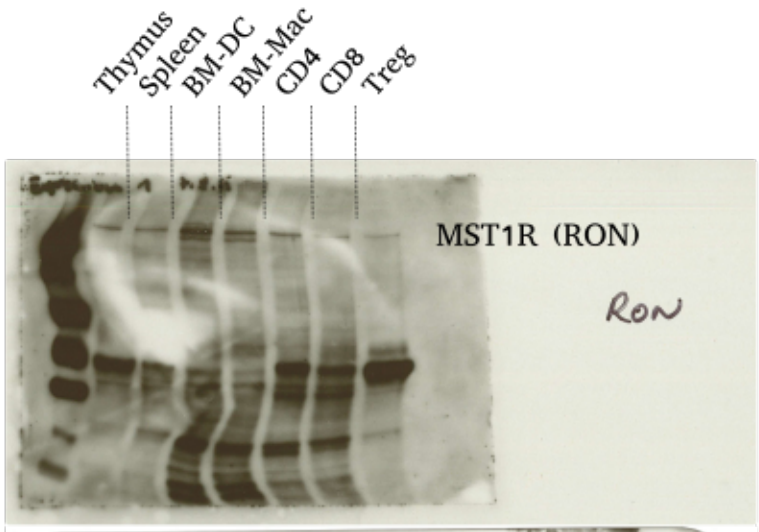


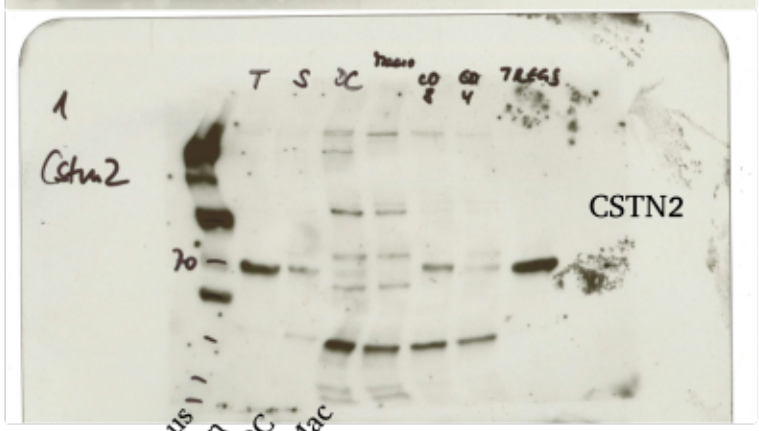


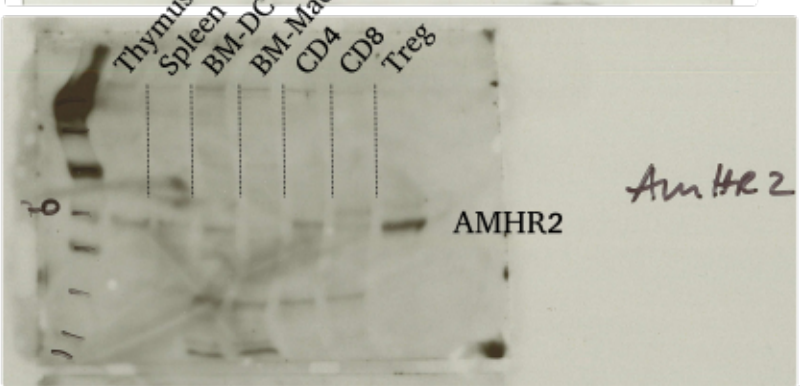


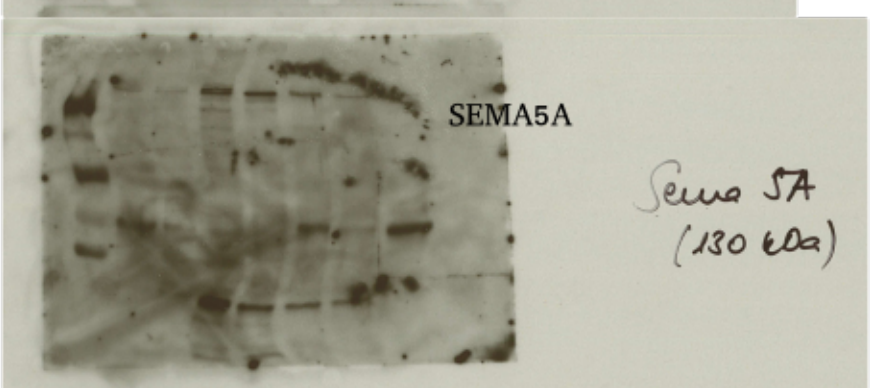


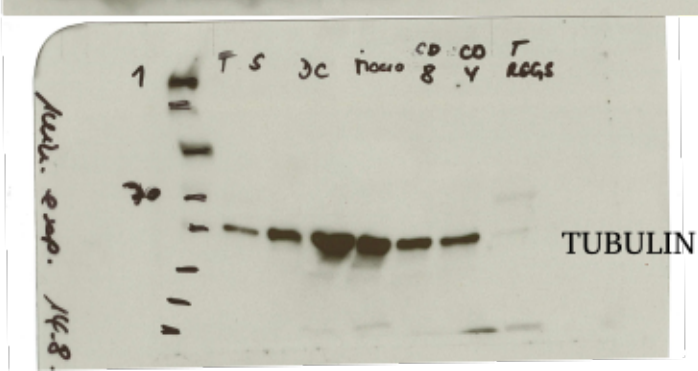

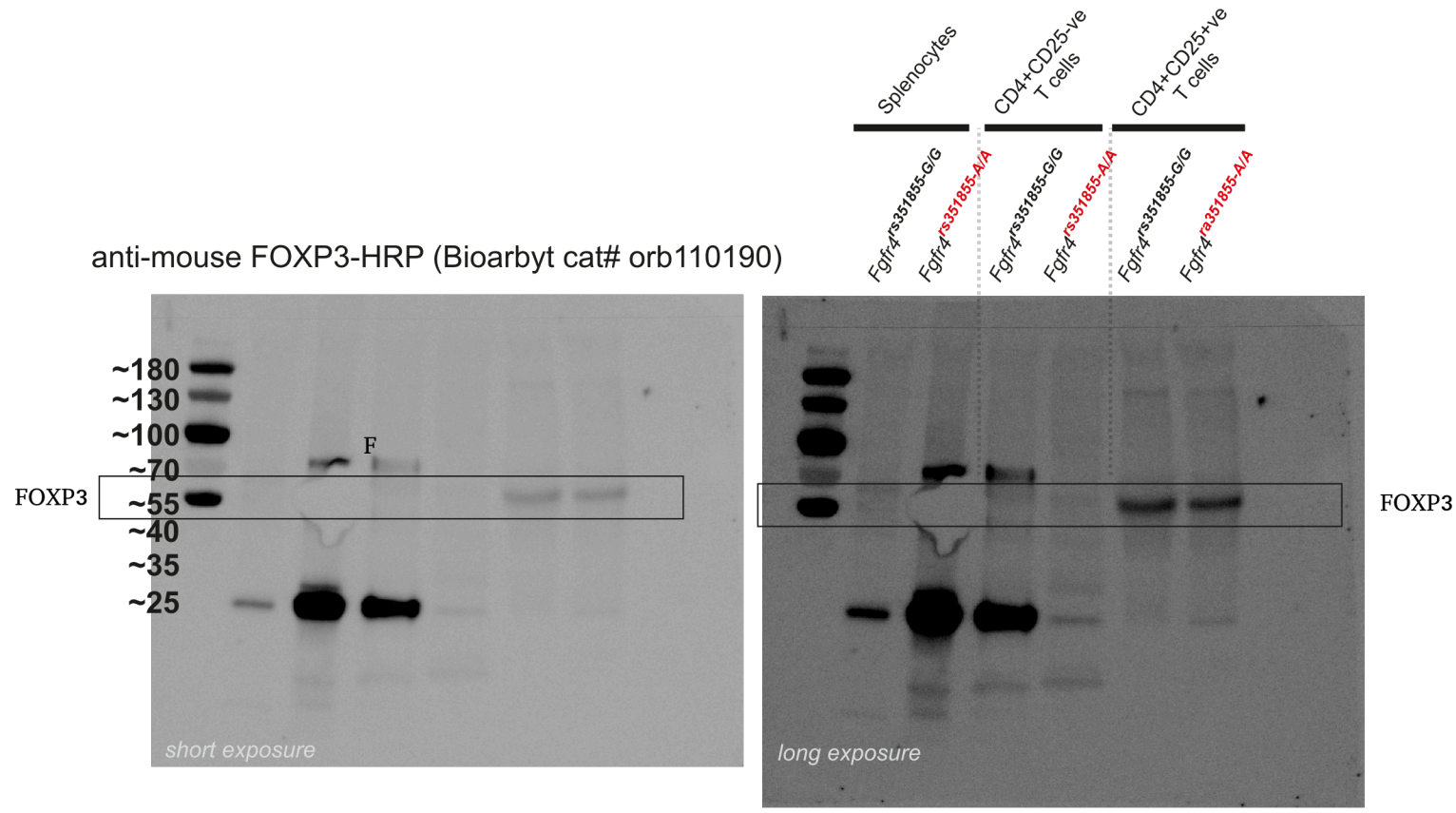
Splenocytes
CD4+CD25-ve T cells
CD4+CD25+ve T cells
Fgfr4rs351855-G/G
Fgfr4rs351855-A/A
Fgfr4rs351855-G/G
Fgfr4rs351855-A/A
Fgfr4rs351855-G/G
Fgfr4ra351855-A/A
anti-mouse FOXP3-HRP (Bioarbyt cat# orb110190)
~180
~130
~100
~70
~55
~40
~35
~25
F
FOXP3
short exposure
long exposure
FOXP3

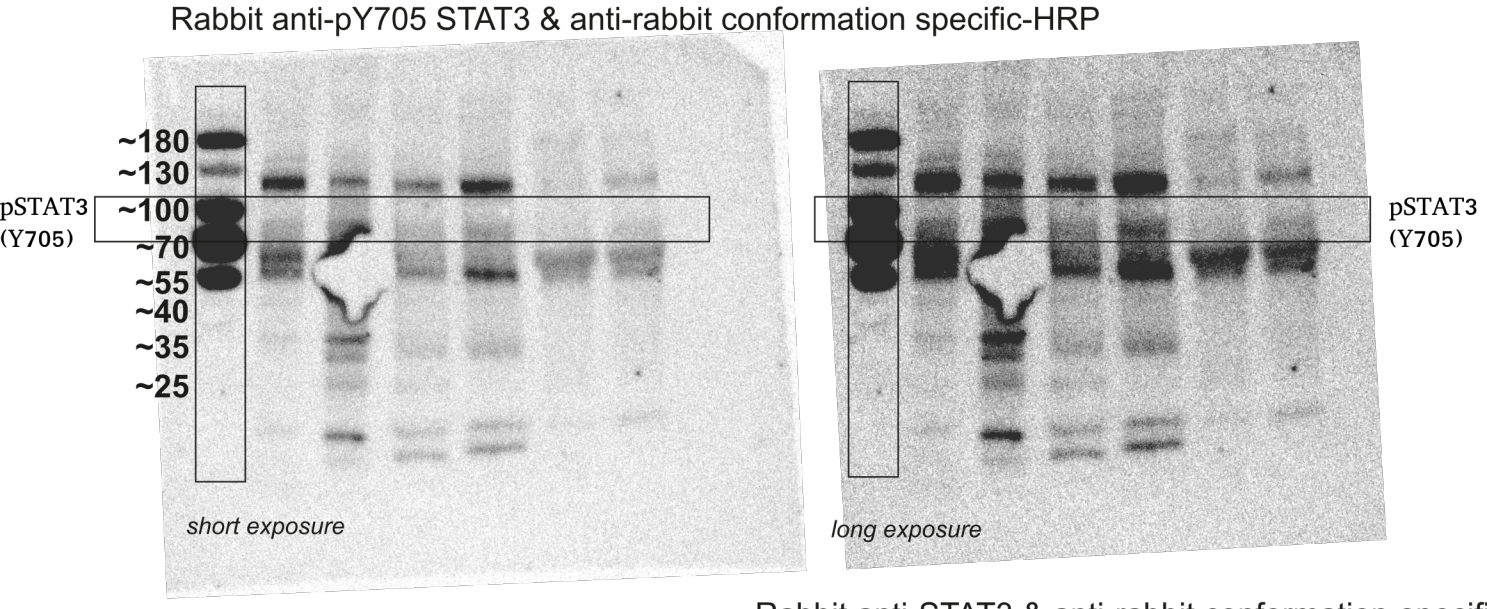
Rabbit anti-pY705 STAT3 & anti-rabbit conformation specific-HRP
~180
~130
~100
~70
~55
~40
~35
~25
pSTAT3 (Y705)
short exposure
long exposure
pSTAT3 (Y705)

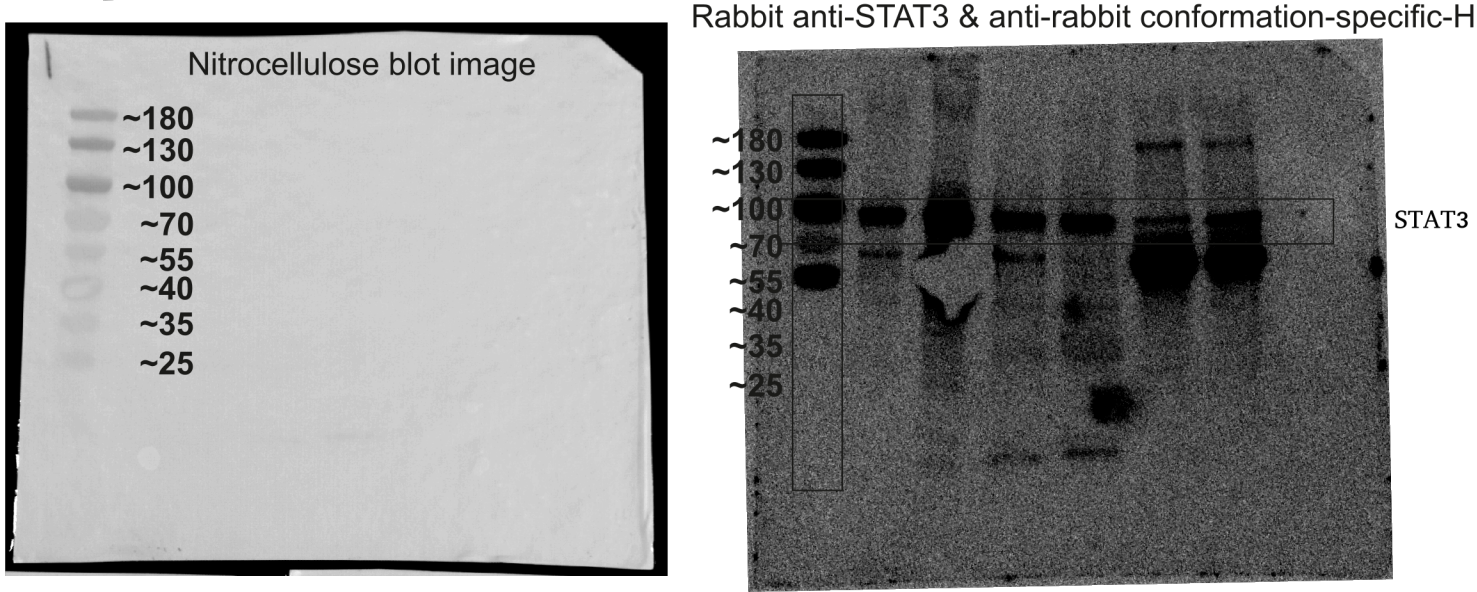
Nitrocellulose blot image
~180
~130
~100
~70
~55
~40
~35
~25
Rabbit anti-STAT3 & anti-rabbit conformation-specific-HRP
~180
~130
~100
~70
~55
~40
~35
~25
STAT3